remote sensing

MDPI

Article

Impact of Aerosols on the Macrophysical and Microphysical Characteristics of Ice-Phase and Mixed-Phase Clouds over the Tibetan Plateau

Shizhen Zhu [1,2], Ling Qian [3], Xueqian Ma [2], Yujun Qiu [1,*], Jing Yang [1], Xin He [1], Junjun Li [1], Lei Zhu [1], Jing Gong [2] and Chunsong Lu [1]

[1] Collaborative Innovation Center on Forecast and Evaluation of Meteorological Disasters, Key Laboratory for Aerosol-Cloud-Precipitation of China Meteorological Administration, Nanjing University of Information Science and Technology, Nanjing 210044, China; 20211203040@nuist.edu.cn (S.Z.); jing.yang@nuist.edu.cn (J.Y.); 20201103005@nuist.edu.cn (X.H.); lijunjun1031@nuist.edu.cn (J.L.); liamzhu2018@nuist.edu.cn (L.Z.); clu@nuist.edu.cn (C.L.)

[2] Meteorological Disaster Prevention Technology Center in Qinghai Province, Xining 810001, China; moblflyqxm@126.com (X.M.); wqc105@163.com (J.G.)

[3] East China Air Traffic Management Bureau, Civil Aviation Administration of China, Shanghai 200335, China; kuangliyong_hd@caac.gov.cn

* Correspondence: qyj@nuist.edu.cn

Abstract: Using CloudSat/CALIPSO satellite data and ERA5 reanalysis data from 2006 to 2010, the effects of aerosols on ice- and mixed-phase, single-layer, non-precipitating clouds over the Tibetan Plateau during nighttime in the MAM (March to May), JJA (June to August), SON (September to November), and DJF (December to February) seasons were examined. The results indicated the following: (1) The macrophysical and microphysical characteristics of ice- and mixed-phase clouds exhibit a nonlinear trend with increasing aerosol optical depth (AOD). When the logarithm of AOD (lnAOD) was ≤ -4.0, with increasing AOD during MAM and JJA nights, the cloud thickness and ice particle effective radius of ice-phase clouds and mixed-phase clouds, the ice water path and ice particle number concentration of ice-phase clouds, and the liquid water path and cloud fraction of mixed-phase clouds all decreased; during SON and DJF nights, the cloud thickness of ice-phase clouds, cloud top height, liquid droplet number concentration, and liquid water path of mixed-phase clouds all decreased. When the lnAOD was >-4.0, with increasing AOD during MAM and JJA nights, the cloud top height, cloud base height, cloud fraction, and ice particle number concentration of ice-phase clouds, and the ice water path of mixed-phase clouds all increased; during SON and DJF nights, the cloud fraction of mixed-phase clouds and the ice water path of ice-phase clouds all increased. (2) Under the condition of excluding meteorological factors, including the U-component of wind, V-component of wind, pressure vertical velocity, temperature, and relative humidity at the atmospheric pressure heights near the average cloud top height, within the cloud, and the average cloud base height, as well as precipitable water vapor, convective available potential energy, and surface pressure. During MAM and JJA nights. When the lnAOD was ≤ -4.0, an increase in aerosols may have led to a decrease in the thickness of ice and mixed-phase cloud layers, as well as a reduction in cloud water path values. In contrast, when the lnAOD was >-4.0, an increase in aerosols may contribute to elevated cloud base and cloud top heights for ice-phase clouds. During SON and DJF nights, changes in various cloud characteristics may be influenced by both aerosols and meteorological factors.

Keywords: Tibetan Plateau; aerosols; cloud phases; impact effects

Citation: Zhu, S.; Qian, L.; Ma, X.; Qiu, Y.; Yang, J.; He, X.; Li, J.; Zhu, L.; Gong, J.; Lu, C. Impact of Aerosols on the Macrophysical and Microphysical Characteristics of Ice-Phase and Mixed-Phase Clouds over the Tibetan Plateau. *Remote Sens.* **2024**, *16*, 1781. https://doi.org/10.3390/rs16101781

Academic Editor: Alexander Marshak

Received: 21 April 2024
Revised: 11 May 2024
Accepted: 15 May 2024
Published: 17 May 2024

1. Introduction

Aerosols primarily affect the Earth's radiative balance and the climate system through aerosol–radiation interactions and aerosol–cloud interactions (ACIs). According to the

Sixth Assessment Report of the Intergovernmental Panel on Climate Change (IPCC) [1], ACIs are the most uncertain radiative forcing factors and pose a challenging issue in current climate research and prediction [2–5]. ACIs primarily encompass indirect effects, semi-direct effects, and cloud-activation effects [6]. These interactions are influenced by various factors including aerosol types, cloud types, cloud phases, and meteorological conditions [7–14]. Compared to other regions on Earth, the aerosol content over the Tibetan Plateau is relatively low, making clouds and radiation more sensitive to aerosols [15,16]. The ACI over the Tibetan Plateau has significant implications for radiation balance, climate change, and downstream weather and climate [16–18]. Studying the influence of aerosols on different phase clouds over the Tibetan Plateau region can provide beneficial insights for better understanding the mechanisms of ACIs on weather and the climate, reducing the uncertainty of climate predictions over the Tibetan Plateau [16,17].

The cloud phase is primarily controlled by atmospheric dynamics and thermodynamic conditions, and different microphysical processes occur in clouds of different phases. There are differences in ACIs among different cloud phases. Due to the less complex microphysical processes in liquid-phase clouds, which do not involve mixed-phase and ice-phase processes, there have been many research findings on the interaction between aerosols and liquid-phase clouds [9,12,19–28]. Numerous studies have found a negative correlation between cloud droplet size and aerosol concentration in liquid-phase clouds, consistent with the traditional aerosol indirect effect or "Twomey effect" by using satellites, aircraft, ground-based observations, etc. [12,19,20,22,24]. However, some studies have also reported phenomena of the "anti-Twomey effect" [9,11,23], and further research indicated that various meteorological factors can influence the correlation between the cloud droplet size and aerosol concentration [9,11,12,23]. The impact of aerosols on ice-phase clouds largely depends on the major nucleation mechanism. Currently, we have a relatively better understanding of homogeneous nucleation, but there are still many unknown factors regarding heterogeneous nucleation, including the concentration and properties of ice nuclei, the major nucleation mechanisms, and the competition between different mechanisms [29]. Moreover, due to the different impact effects of aerosols on ice clouds, the changes in ice particle size and ice water content (units: mg m^{-3}) are quite complex. The combined effects of aerosol indirect effects and semi-direct effects may result in decreases in both ice particle size and ice water content [30–32]. However, during the heating process, the aerosol activation effect enhanced by convective activity may lead to an increase in ice water content with increasing AOD (aerosol optical depth) [33]. In the presence of ice nuclei, an increase in ice nucleus concentration can also lead to the "Twomey effect" observed in liquid-phase clouds, resulting in more and smaller ice particles [34,35]. However, in heterogeneous nucleation processes, fewer and larger ice particles may also be produced [30]. Mixed-phase clouds consist of liquid water and ice crystals and involve multiple microphysical processes such as collision–coalescence, riming, and deposition. There is currently no consensus on the impact of aerosols on cloud droplet size and precipitation in mixed-phase clouds, with different studies yielding various results [36–42].

The Tibetan Plateau has a fragile and sensitive ecological environment and is a sensitive region to global climate change [43–45]. In the atmosphere surrounding the Tibetan Plateau, there are various types of aerosol source regions with significant spatiotemporal variations [46]. The region's aerosols primarily consist of dust (DU), along with various other types [47]. Among them are DU aerosols, which are a type of absorbing aerosol and can act as both cloud condensation nuclei and ice nuclei. Thus, they can influence the macrophysical and microphysical characteristics of clouds through various effects, including an indirect effect, semi-direct effect, and cloud-activation effect [48–54]. Consequently, the impact of dust aerosols on clouds is highly complex. Some scholars have studied the impact of aerosols on clouds in plateau regions, and the research indicates that the cloud phase, cloud type, diurnal and nocturnal differences, liquid water path (LWP), convective available potential energy (CAPE), moisture convergence/divergence, terrain uplifting, aerosol particle size, and other factors all have important influences on ACIs [25,52,55–58].

Hua et al. [55] found that aerosols in plateau regions primarily affect ice clouds, with minimal impact on water clouds. The impact on ice clouds mainly manifests as a reduction in daytime ice particle effective radius (IER) and an increase in the nighttime ice water path (IWP) and cloud optical thickness. Zhao et al. [25] found spatial differences in the impact of aerosols on liquid-phase clouds, where in the southern region the impact of aerosols on liquid-phase clouds mainly depends on LWP and CAPE, while in the northern region the impact of aerosols on liquid-phase clouds is more likely to be related to a larger aerosol particle size. Yuan et al. [58] found that in the southeastern part of the Tibetan Plateau during summer, increased aerosols can lead to an increase in the cloud frequency under moisture convergence or terrain uplifting conditions; when moisture conditions are divergent, increased aerosols can lead to a decrease in cloud frequency, but the increase in sulfate (SU) aerosols can significantly enhance hygroscopic growth, promoting cloud formation and development. Some researchers have also studied the impact of dust aerosols on clouds and obtained conflicting results for different types of clouds. For convective clouds, Liu et al. [18,59] found that with increasing AOD, DU aerosols will reduce the cloud droplet effective radius and increase the cloud optical depth, LWP, and ice water path (IWP). Pan et al. [52] found that the influence of DU aerosols on cirrus in the plateau results in a smaller IWP, ice water content, IER, and ice particle number concentration (INC). These different results may be due to different dominant effects. Although many studies have delved into ACIs over the Tibetan Plateau, it is still challenging to provide a definitive explanation for the underlying physical mechanisms due to the complexity of interactions between aerosols and different cloud phases.

Previous long-term studies on the interaction between aerosols and different cloud phases have mostly relied on passive remote sensing satellite data [9,21,25,56,57,60,61]. Due to the inherent limitations of passive observations, only relevant information at the cloud top can be detected, making it difficult to understand the vertical structure of clouds. Based on active remote sensing, the CloudSat and CALIPSO satellites have accumulated observational data on the vertical distribution of clouds and aerosols, cloud types, and cloud phases [32,62–64]. Additionally, previous studies based on the satellites have mainly used monthly mean data to investigate the correlation between aerosols and different cloud phases, primarily reflecting their relationship with long-term time scales, lacking real-time feedback on their interaction at short-term time scales. This study took advantage of the CloudSat/CALIPSO satellite observational dataset to investigate the impact of aerosols on single-layer, non-precipitating, ice-phase clouds and mixed-phase clouds using data from 19 June 2006 to 31 December 2010, aiming to provide a reference for a further understanding of ACIs.

2. Data and Methods

2.1. Study Area

The Tibetan Plateau, known as the "Roof of the World" and "The Third Pole," is the highest plateau in the world. It extends from the Pamir Plateau in the west to the Hengduan Mountains in the east, bordered by the Himalayas to the south and the Kunlun, Altun, and Qilian mountains to the north. With its rugged terrain and an average altitude exceeding 4000 m, the plateau is the origin of many major rivers in East, Southeast, and South Asia, and is a gathering place for glaciers, lakes, and wetlands in Asia, earning it the nickname "Asian Water Tower". It is a region highly sensitive to climate change [65]. Our study focused on the central part of the Tibetan Plateau, within the range of 25°N–40°N and 70°E–105°E, specifically the region enclosed by the black solid line in Figure 1, where the altitude is above 2000 m.

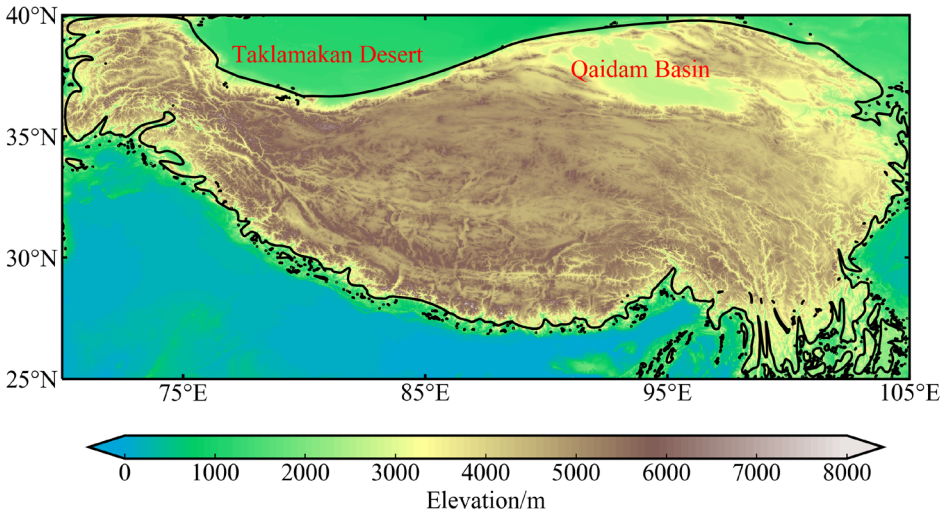

Figure 1. Topographic map of the Tibetan Plateau. The black solid line represents the 2 km topographic contour, which encloses the study area.

2.2. Data Sources

This study utilized the Modern-Era Retrospective Analysis for Research and Applications, Version 2 (MERRA-2) reanalysis data M2TMNXAER monthly average product from June 2006 to December 2010, the CloudSat/CALIPSO satellite orbital data from 19 June 2006 to 31 December 2010, and the European Centre for Medium-Range Weather Forecasts (ECMWF) Reanalysis v5 (ERA5) hourly product (https://cds.climate.copernicus.eu/cdsapp#!/dataset/, accessed on 1 December 2023). The parameters used are shown in Table 1.

Utilizing the MERRA-2 reanalysis data M2TMNXAER monthly average product to calculate the seasonal averages of DU, SU, organic carbon (OC), black carbon (BC), sea salt (SS) aerosol, and total aerosol optical depth (AOD) to analyze the seasonal distribution characteristics of aerosols. In analyzing the correlation between aerosols and the macrophysical/microphysical characteristics of clouds and meteorological factors, aerosol data were derived from the CALIPSO satellite's L2_05kmAPro_V4 product Extinction_Coefficient_532 integrated to obtain AOD. Macrophysical characteristics of cloud data came from CloudSat satellite's 2B-CLDCLASS product, including cloud top height (CTH) and cloud base height (CBH). Cloud thickness (CT) is calculated by the difference between CTH and CBH, and cloud fraction (CF) is calculated by using Equation (1) in Section 2.5. Microphysical characteristics data came from the 2B-CWC-RO product, including the liquid droplet/ice particle effective radius (LER/IER), liquid droplet/ice particle number concentration (LNC/INC), LWP/IWP. Meteorological factors data were obtained from the ERA5 hourly product, including the U-component of wind (U); V-component of wind (V); pressure vertical velocity (PVV); temperature (T); relative humidity (RH) at the atmospheric pressure heights near the average CTH, within the cloud, and the average CBH; precipitable water vapor (PWV); CAPE; and surface pressure (SP). The definitions and physical meanings of various cloud macrophysical characteristics of clouds, microphysical characteristics of clouds, and meteorological factors are shown in Tables S1–S3, respectively.

Table 1. MERRA-2, CALIPSO, CloudSat, and ECMWF data products used in this study.

Data	Observation Wavelength	Product	Parameter	Spatial Resolution	Temporal Resolution	Period	Usage
MERRA-2	/	M2TMNXAER	Black Carbon AOD, Dust AOD, Organic Carbon AOD, Sea Salt AOD, Sulfate AOD, Total AOD	0.625° × 0.5° horizontal	Monthly	June 2006–December 2010	Analyze the distribution characteristics of aerosols
CALIPSO	532 and 1064 nm	L2_05kmAPro_V4	Extinction_Coefficient_532, Extinction_Coefficient_Uncertainty_532, CAD_Score, Extinction_QC_Flag_532, Atmospheric_Volume_Description	5 × 5 km horizontal; 0.06 km from −0.5 to 20.2 km, 0.18 km from 20.2 to 30.1 km vertical	Ground tracks repeat every 16 days	19 June 2006–31 December 2010	Calculate AOD and analyze the correlation between AOD and cloud macrophysical/microphysical characteristics
CloudSat	3.2 mm	2B-CLDCLASS /2B-CLDCLASS-LIDAR	CTH, CBH, Cloud Layer, Precip Flag, Cloud Phase	1.3 × 1.7 km horizontal; 10 layers vertical	Ground tracks repeat every 16 days	19 June 2006–31 December 2010	Analyze the correlation between AOD and cloud macrophysical characteristics
		2B-CWC-RO	LER, IER, LNC, INC	1.3 × 1.7 km horizontal; 0.24 km vertical	Ground tracks repeat every 16 days	19 June 2006–31 December 2010	Analyze the correlation between AOD and cloud microphysical characteristics
			LWP, IWP	1.3 × 1.7 km horizontal			
ECMWF	/	ERA5	U, V, PVV, T, RH	0.25° × 0.25° horizontal; 37 pressure levels from 1000 hPa to 1 hPa	Hourly	19 June 2006–31 December 2010	Analyze the correlation between AOD, cloud macrophysical/microphysical characteristics, and meteorological factors
			PWV, CAPE, SP	0.25° × 0.25° horizontal			

2.3. Data Quality Control

The quality control of aerosol Extinction_Coefficient_532 in CALIPSO data involved filtering based on the following criteria: Extinction_Coefficient_Uncertainty_532 < 10 km^{-1}, $-100 \leq$ CAD_Score ≤ -70, Extinction_QC_Flag_532 value of 0 or 1, and Atmospheric_Volume_Description values converted to 16-bit binary format with the first to third bits being 3 [66]. Unlike passive remote sensing, which acquires AOD during the day by scattering solar radiation, the CALIPSO satellite, being an active remote sensing instrument, can emit laser signals to obtain AOD during both day and night. However, due to the noise in the signal caused by solar radiation during the day, the accuracy of AOD measurements at night is significantly higher [67]. Therefore, this paper only selected nighttime data.

2.4. Data Sample Selection

To achieve spatial data matching, the spatial matching method developed by Jiang et al. [7] was utilized. Initially, a $1^\circ \times 1^\circ$ grid box centered around each CloudSat profile was established. Subsequently, all the CALIPSO aerosol profiles within this grid were identified, and the aerosol extinction coefficient for each profile was quality controlled and then integrated vertically to obtain the AOD. The matched AOD is the average of all AODs within the $1^\circ \times 1^\circ$ grid box.

To eliminate the influence of overlapping multi-layer clouds and precipitation, this study selected only single-layer, non-precipitating clouds. For each grid box in the CloudSat data, macrophysical and microphysical characteristics of single-layer, non-precipitating clouds of different phases were extracted and averaged. The determination of cloud layers, precipitation presence, and cloud phase relied on CloudSat's Cloud Layer, Precip_flag, and cloud phase parameters, respectively. Since CALIPSO data were selected only for nighttime, the CALIPSO and CloudSat satellites predominantly cross the Tibetan Plateau between 0100 and 0300 China Standard Time (CST). Correspondingly, ERA5 reanalysis meteorological data at 0200 CST, averaging various meteorological factors within each $1^\circ \times 1^\circ$ grid, were used to match with cloud characteristics and AOD data.

The determination of cloud phase in the 2B-CLDCLASS-LIDAR product is mainly based on the differences in microphysical characteristics and optical properties between ice particles and liquid droplets (https://www.cloudsat.cira.colostate.edu/cloudsat-static/info/dl/2b-cldclass-lidar/2B-CLDCLASS-LIDAR_PDICD.P1_R05.rev0_.pdf, accessed on 5 January 2023). The determination process was as follows: Because ice-phase clouds and liquid-phase clouds have different degrees of attenuation of lidar signals, lidar signals can penetrate ice-phase cloud layers for several kilometers, but are typically attenuated within a few hundred meters by liquid-phase cloud layers. Therefore, the sensitivity of CloudSat's cloud radar and CALIPSO's lidar to ice particles and liquid droplets was used to determine the cloud phase. First, by locating a strong signal that increases and then decreases (due to attenuation), the presence of liquid-phase cloud layers can be detected [68], and this information was combined with the jointly inverted cloud droplet number concentration from CloudSat and CALIPSO to improve the identification of liquid-phase cloud layers. Then, the positions of liquid-phase cloud layers identified by lidar and the maximum reflectivity factor of the cloud layer detected by cloud radar were used to distinguish between supercooled liquid-phase cloud layers and mixed-phase cloud layers. Finally, a multi-stage logic discrimination scheme based on liquid-phase cloud layer detection, cloud top temperature, cloud base temperature, temperature-related radar reflectivity factor thresholds [69], and integrated attenuated backscatter coefficients was used to determine the cloud phase, classifying it into three phases: ice phase, mixed phase, and liquid phase.

2.5. CF Calculation

Using the method of Fang et al. [70], CF was calculated by first dividing the Tibetan Plateau area into several grid points of $1^\circ \times 1^\circ$ in latitude and longitude. Then, the total

CF and the CF of different phases (CF(i, j)) for each grid point in different seasons were calculated as follows:

$$CF(i,j) = \frac{1}{N(i,j)} \sum_{p=1}^{N(i,j)} n_{p,cloud}(i,j), \quad (1)$$

where N represents the number of satellite trajectory grid points in the 1°×1° latitude and longitude grid (i, j). If clouds/specific phase clouds are found in the vertical profile, then n = 1. The seasonal average CF calculated is the ratio of cloud profile occurrences to the total profile count within a 1° × 1° grid for a specific season. According to calculations, from 19 June 2006 to 31 December 2010, within the range of 25°N–40°N and 70°E–105°E, due to the unevenness of polar satellite observations, the total number of profiles within different grids ranged from 0 to 5121. The average number of profiles across all grids was 2460. To avoid the overestimation of CF due to sparse data within a grid, this study only selected grids with a total profile count greater than 50 for CF calculation.

In the correlation analysis, the CF for each cloud phase was derived by dividing the number of profiles for that phase by the total number of profiles within the 1° × 1° grid on the orbit, as selected in Section 2.3 for data sample selection.

2.6. Correlation Analysis

The partial correlation coefficient quantifies the linear correlation between two variables among multiple variables while controlling for the influence of other variables, establishing the intrinsic linear relationship between the two. Considering three variables, x_1, x_2, and x_3, and excluding the influence of one variable to calculate the partial correlation coefficient between the other two is known as the first-order partial correlation coefficient. The definition formula is as follows [71]:

$$\rho_{23\cdot1} = \frac{\rho_{23} - \rho_{12}\rho_{13}}{\sqrt{1-\rho_{12}^2}\sqrt{1-\rho_{13}^2}}, \quad (2)$$

where ρ_{23}, ρ_{12}, and ρ_{13} represent the Spearman correlation coefficients between the pairs of variables, and $\rho_{23\cdot1}$ is the partial correlation coefficient between x_2 and x_3, controlling for variable x_1.

For n (n > 3) variables, x_1, x_2, …, x_n, the computation of the kth-order ($k \leq n-2$) partial correlation coefficient between any two variables x_i and x_j is as follows:

$$\rho_{ij\cdot12\cdots k} = \frac{\rho_{ij\cdot12\cdots(k-1)} - \rho_{ik\cdot12\cdots(k-1)}\rho_{jk\cdot12\cdots(k-1)}}{\sqrt{1-\rho_{ik\cdot12\cdots(k-1)}^2}\sqrt{1-\rho_{ik\cdot12\cdots(k-1)}^2}}, \quad (3)$$

where $\rho_{ij\cdot12\ldots k}$ represents the kth-order partial correlation coefficient between x_i and x_j. Additionally, $\rho_{ij\cdot12\ldots(k-1)}$, $\rho_{ik\cdot12\ldots(k-1)}$, and $\rho_{jk\cdot12\ldots(k-1)}$ refer to the (k − 1)th-order partial correlation coefficients for x_i and x_j, x_i and x_k, and x_j and x_k, respectively.

In assessing how aerosols influence cloud macrophysical and microphysical characteristics, to exclude the influence of meteorological factors, this study calculated the total correlation coefficients between AOD and the macrophysical/microphysical characteristics of clouds, and the partial correlation coefficients between AOD and the macrophysical/microphysical characteristics of clouds, both when controlling for various single meteorological factors and when controlling for all meteorological factors simultaneously. If the partial and total correlation coefficients are consistent in sign and are all significant, it indicates that the correlation between aerosols and cloud characteristics is primarily due to aerosols. If the total correlation coefficient is significant but the partial and total coefficients are opposite in sign, it suggests that the correlation is mainly influenced by meteorological factors. If the total and partial correlation coefficients are consistent in sign and the total correlation is significant but the partial is not, it implies that the correlation is caused by both aerosols and meteorological factors [7,57,72]. The meteorological variables

considered in the partial correlation analysis included the various types listed in Table 1 of the ERA5 dataset.

3. Results

3.1. Distribution Characteristics of Aerosols and Clouds

The AOD is a proxy for the aerosol content in the whole atmospheric column, with higher values indicating a greater aerosol content [73]. According to MERRA-2 reanalysis data from 2006 to 2010, the seasonal average AOD over the Tibetan Plateau was as follows: ranging from 0.08 to 0.55 in MAM (March to May), ranging from 0.06 to 0.58 in JJA (June to August), ranging from 0.04 to 0.46 in SON (September to November), and ranging from 0.03 to 0.42 in DJF (December to February). Across all seasons, the AOD exhibited a decreasing trend from north to south, with a notable area of high AOD values situated in the Qaidam Basin. The Taklamakan Desert, situated in the northern part of the Tibetan Plateau, frequently encounters DU events during the MAM and JJA seasons [74–76], significantly influencing the AOD over the Tibetan Plateau [47,77]. DU aerosols exhibit a seasonal and regional distribution pattern similar to the AOD, while other types of aerosols are predominantly found in the southern and eastern regions of the plateau, as depicted in Figure 2. In the plateau area, the average AOD values during MAM, JJA, SON, and DJF were 0.19, 0.14, 0.09, and 0.08, respectively. It is noteworthy that the AOD values in MAM and JJA were significantly higher than those in SON and DJF.

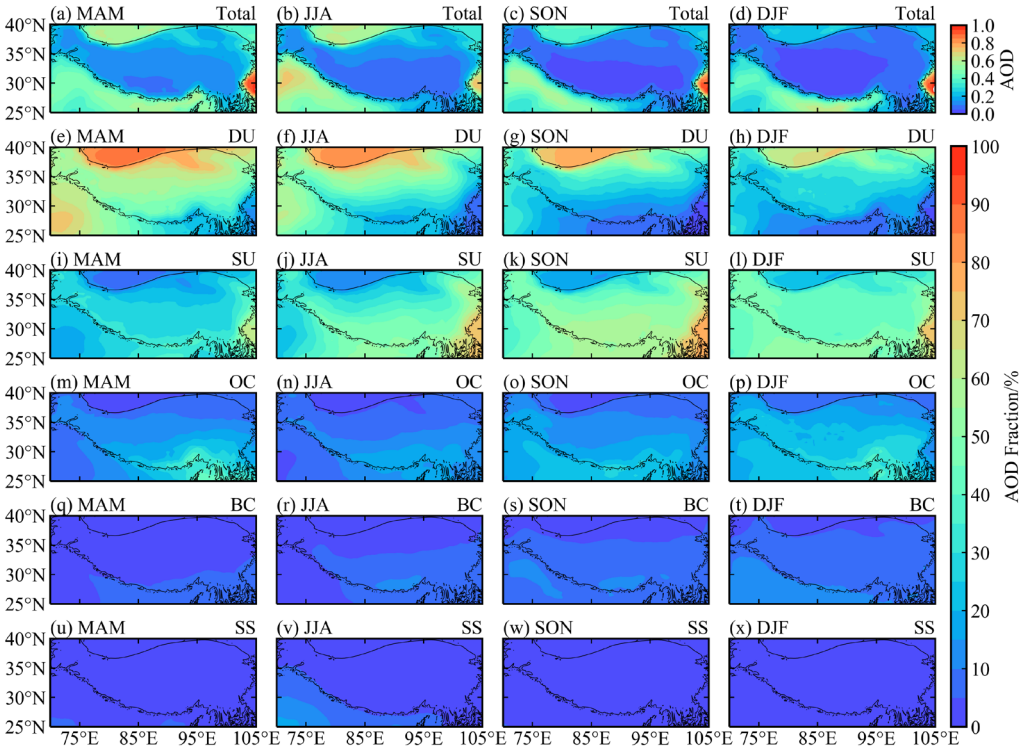

Figure 2. Distribution of the total aerosol optical depth (Total AOD) and the ratio of different types of AOD to total AOD over the Tibetan Plateau for each season from 2006 to 2010, based on MERRA-2 data. (**a**) March to May (MAM), (**b**) June to August (JJA), (**c**) September to November (SON), (**d**) December to February (DJF) total AOD; (**e**–**h**) ratio of dust (DU) aerosol optical depth to total AOD; (**i**–**l**) same as (**e**–**h**) for sulfate (SU) aerosols; (**m**–**p**) same as (**e**–**h**) for organic carbon (OC) aerosols; (**q**–**t**) same as (**e**–**h**) for black carbon (BC) aerosols; (**u**–**x**) same as (**e**–**h**) for sea salt (SS) aerosols. The black solid line represents the 2 km topographic contour.

Over the Tibetan Plateau, the major aerosol components are DU, SU, and OC, collectively constituting over 90% of the total AOD throughout the year and in each season. In

MAM, DU aerosols comprise the largest proportion over the plateau, accounting for 46%, followed by SU aerosols at 30%, and subsequently, OC, BC, and SS aerosols. In seasons other than MAM, SU aerosols have the highest proportion, followed by DU, OC, and SS. In JJA, SU and DU aerosols have comparable proportions, accounting for 43% and 41%, respectively. In SON and DJF, due to reduced DU, the proportion of SU aerosols is significantly higher than other types, accounting for 54% and 47%, respectively.

According to CloudSat satellite data, the CF over the Tibetan Plateau shows clear seasonal variations, as illustrated in Figure 3. The total CF decreases progressively in MAM, JJA, SON, and DJF, with average values of 40%, 39%, 32%, and 31%, respectively. The CF of ice-phase clouds follows a similar pattern, decreasing in the order of MAM, DJF, JJA, and SON, with averages of 32%, 26%, 22%, and 20%, respectively. The CF of mixed-phase and liquid-phase clouds decreases in the order of JJA, SON, MAM, and DJF, with the average CF being 20%, 11%, 10%, and 5%, and 3%, 2%, 1%, and 0.5%, respectively. Due to the high altitude of the plateau, ice- and mixed-phase clouds predominate. On average, ice-phase clouds had the highest CF across all seasons, followed by mixed-phase clouds, while liquid-phase clouds had the lowest CF.

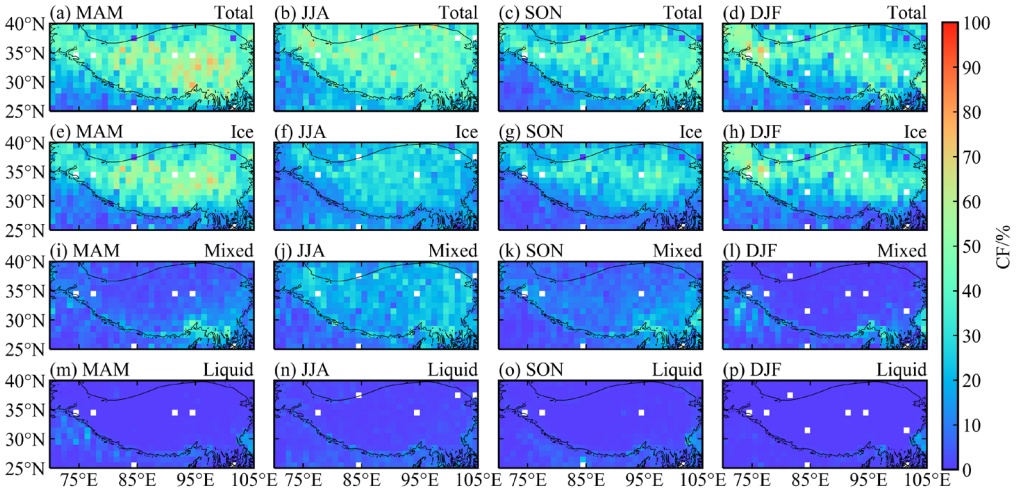

Figure 3. Distribution of total cloud fraction (CF) and CF of different phases over the Tibetan Plateau for each season from 2006 to 2010 based on CloudSat data. (**a**) MAM, (**b**) JJA, (**c**) SON, (**d**) DJF total CF; (**e**–**h**) same as (**a**–**d**) for ice-phase clouds; (**i**–**l**) same as (**a**–**d**) for mixed-phase clouds; (**m**–**p**) same as (**a**–**d**) for liquid-phase clouds. The black solid line represents the 2 km topographic contour.

3.2. Correlation between Aerosols and Cloud Characteristics

Based on the analysis of aerosol and cloud distribution characteristics in Section 3.1, the Tibetan Plateau region had a higher proportion of DU aerosols during MAM and JJA, which decreased in SON and DJF, with SU aerosols having the highest proportion. Clouds over the plateau region were majorly ice-phase and mixed-phase. Moreover, in the data sample selection of Section 2.3, only nighttime AOD data from CALIPSO were chosen. To exclude the effects of multi-layer cloud overlap and precipitation, only single-layer non-precipitating cloud characteristic data were selected. Therefore, this paper separately analyzed the correlation between nighttime aerosols and single-layer non-precipitating ice-phase and mixed-phase clouds for the MAM and JJA, and the SON and DJF seasons, respectively.

Due to the low AOD values in the plateau region, with most values concentrated at the lower end of the AOD, for ease of analysis the AOD values were first converted to logarithms. Then, using log values (lnAOD) at intervals of 0.25, all samples were categorized into several groups. The probability density distributions of lnAOD during the nighttime for MAM and JJA and SON and DJF are shown in Figures S1 and S2, respectively. To mitigate the impact of the uneven sample distribution, only categories with more than

3% of the samples were selected. Due to the non-normal distribution of the data, the correlation coefficients used in this study are all Spearman correlation coefficients.

3.2.1. Macrophysical Characteristics of Clouds

During the nighttime of MAM and JJA, the macrophysical characteristics of single-layer non-precipitating ice-phase and mixed-phase clouds over the Tibetan Plateau showed a nonlinear trend with increasing lnAOD (as shown in Figure 4). As the AOD increased, the CBH of ice-phase clouds showed a significant increase, while that of mixed-phase clouds changed little. The CT of both types of clouds exhibited opposite trends within the low and high ranges of AOD, both showing a characteristic of first decreasing and then increasing with a rising AOD. Additionally, the CF of ice-phase and mixed-phase clouds exhibited opposite trends with increasing AOD, the former increased and was more pronounced at higher AOD values, while the latter decreased and was more evident at lower AOD values. The boundary was approximately marked by lnAOD = −4.0 (AOD = 0.018) because the CT and CF of ice-phase clouds and mixed-phase clouds changed with the lnAOD in the interval where the lnAOD value was less than −4.0 and in the interval where the lnAOD value was greater than −4.0. As the dividing point, this dividing point is not unique. Since the focus of the article was to study the changing trend mentioned above, there is no special explanation for taking the lnAOD equal to −4.0 as the dividing point.

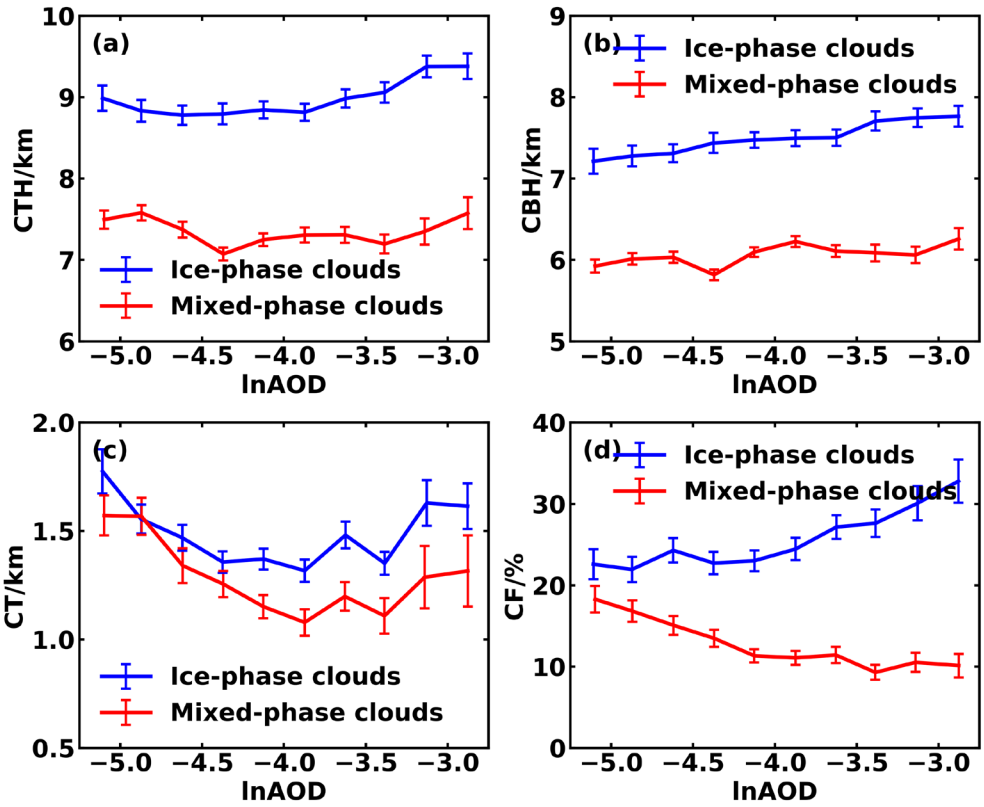

Figure 4. Trends of macrophysical characteristics of single-layer non-precipitating ice-phase and mixed-phase clouds over the Tibetan Plateau during the nighttime in MAM and JJA within different logarithmic aerosol optical depth (lnAOD) intervals with changing lnAOD based on CloudSat and CALIPSO data: (**a**) cloud top height (CTH), (**b**) cloud base height (CBH), (**c**) cloud thickness (CT), (**d**) cloud fraction (CF). The error was calculated as $\frac{s}{\sqrt{n-2}}$, where n is the number of samples for each macrophysical characteristic within each lnAOD interval, and s is the standard deviation.

In the low AOD range (lnAOD ≤ -4.0), as the AOD increased, the CTH of ice-phase clouds showed a slight decreasing trend, while the CBH increased. The CTH of mixed-phase clouds tended to decrease and the CBH changed little, with both ice-phase and

mixed-phase clouds showing a thinning trend. Linear fitting and significance testing of the trends in cloud characteristic changes were conducted separately for cases of lnAOD ≤ -4.0 and lnAOD > -4.0, as indicated in Table S4. According to Table S4, within the lower AOD range, the CT of ice-phase and mixed-phase clouds showed a decreasing trend as the AOD increased, with both passing the 95% significance test. For each unit change in the lnAOD, the CT decreased at rates of 0.41 km and 0.47 km, respectively. Combining the trends of CF changes under two phase states, the CF of ice-phase clouds changed minimally, whereas for mixed-phase clouds, the CF significantly decreased at a rate of 7.05% for each unit change in the lnAOD. This indicates that when the aerosol content is low the vertical development of both ice-phase and mixed-phase clouds weakens with the increase in aerosols. Meanwhile, the horizontal development of ice-phase clouds remains essentially unchanged, while the horizontal development of mixed-phase clouds also weakens. This may be related to the semi-direct effect of DU aerosols, which are the main aerosol types over the Tibetan Plateau. Compared to ice-phase clouds, mixed-phase clouds have higher temperatures, and the heating effect of DU aerosols is more pronounced. With the increase in DU aerosols, more cloud droplets evaporate, leading to thinner clouds and a reduced CF [78].

In the high AOD range (lnAOD > -4.0), as the AOD increased, the CTH and CBH of ice-phase clouds rose and the CT and CF increased. For mixed-phase clouds, the CTH increased and the CT became thicker, while the CBH and CF showed little change. According to Table S4, for each unit change in the lnAOD, the CTH, CBH, and CF of ice-phase clouds significantly increased at rates of 0.61 km, 0.31 km, and 7.9%, respectively. The CT of ice-phase clouds and both the CTH and CT of mixed-phase clouds also increased, but not significantly. This indicates that when the aerosol content is high, with the increase in aerosols, the development of ice-phase clouds is enhanced both vertically and horizontally. This may be due to the fact that at high AOD levels, DU aerosols, acting as ice nuclei, enhance the formation of ice crystals, thereby strengthening the indirect effects and cloud-activation effects [79,80]. In MAM and JJA, the Tibetan Plateau's aerosols are primarily DU, which can be lifted to the top of the troposphere [81]. Froyd et al. [79] demonstrated that DU aerosols can induce cirrus clouds in all seasons outside the tropics and dominate the formation of cirrus clouds in the Northern Hemisphere. Shen et al. [80] also found that long-range transported DU aerosols can act as ice nuclei. They noted that when the concentration of ice crystals in the cloud is less than 100 L^{-1}, the DU-related heterogeneous nucleation process dominates in the formation of cirrus clouds, leading to an increased cirrus CF. Additionally, for DU-polluted convective clouds over the plateau region, the greater the AOD, the higher the development of convective clouds [18].

Compared to MAM and JJA, during SON and DJF (as shown in Figure 5), when the AOD increased, the CTH and CBH of non-precipitating, single-layer ice-phase and mixed-phase clouds over the Tibetan Plateau changed little, while the CT and CF exhibited irregular trends with an increasing AOD. To correspond with MAM and JJA, the trends in CT and CF change within low AOD ranges (lnAOD ≤ -4.0) and high AOD ranges (lnAOD > -4.0) were analyzed separately. Similar to MAM and JJA, with lnAOD $= -4.0$ as the boundary, the CT of ice-phase and mixed-phase clouds in SON and DJF generally showed a trend of first decreasing and then increasing, while the CF changed little within the low AOD range and tended to increase within the high AOD range. According to Table S5, within the low AOD range, the CTH of mixed-phase clouds and the CT of ice-phase clouds both significantly decreased; in the high AOD range, only the CF of mixed-phase clouds significantly increased at a rate of 7.88% for each unit change in lnAOD. This may be due to the decrease in the proportion of DU aerosols and the predominance of SU aerosols in SON and DJF, which weakens the semi-direct effect of aerosols. Moreover, the strong hygroscopicity of SU aerosols, serving as effective cloud condensation nuclei [82,83], could be the reason for the increase in CF of mixed-phase clouds within the high AOD range.

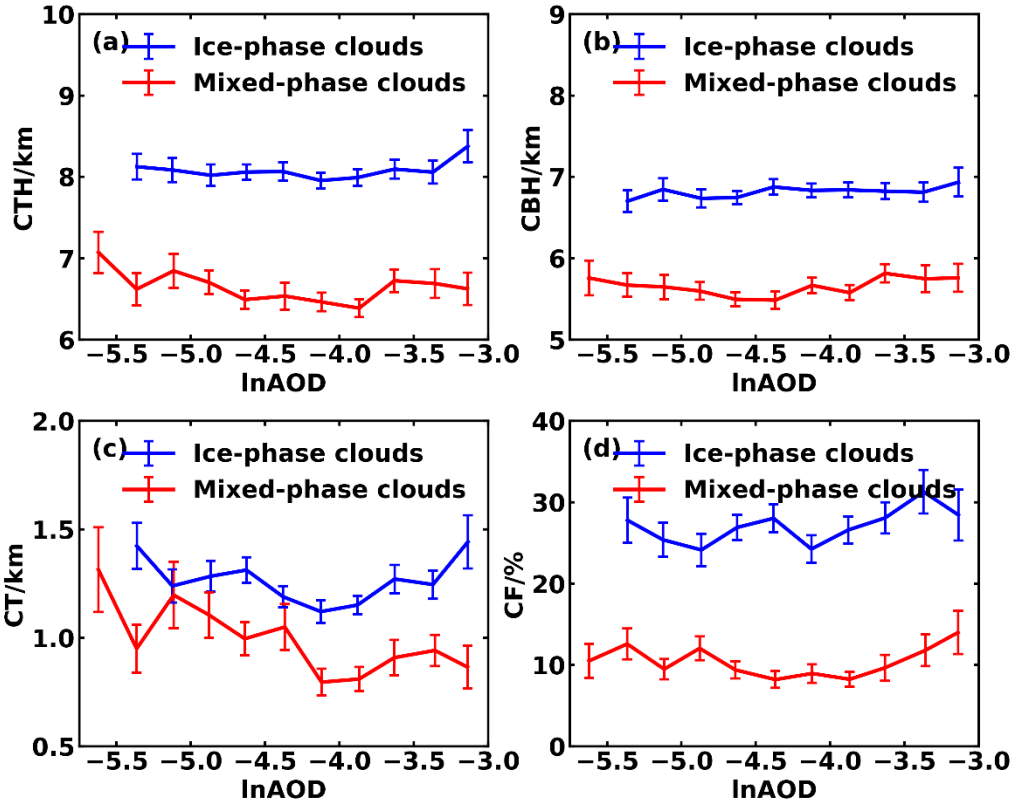

Figure 5. Trends of macrophysical characteristics of single-layer non-precipitating ice-phase and mixed-phase clouds over the Tibetan Plateau during the nighttime in SON and DJF within different logarithmic aerosol optical depth (lnAOD) intervals with changing lnAOD based on CloudSat and CALIPSO data: (**a**) cloud top height (CTH), (**b**) cloud base height (CBH), (**c**) cloud thickness (CT), (**d**) cloud fraction (CF). The error was calculated as $\frac{s}{\sqrt{n-2}}$, where n is the number of samples for each macrophysical characteristic within each lnAOD interval, and s is the standard deviation.

3.2.2. Microphysical Characteristics of Clouds

During MAM and JJA nights, the variations in microphysical characteristics of single-layer non-precipitating ice-phase and mixed-phase clouds with AOD are shown in Figure 6. In the low AOD range, ice-phase clouds exhibited a clear decreasing trend in the IER, INC, and IWP with an increasing AOD. According to Table S6, for each unit change in the lnAOD, the IER, INC, and IWP of ice-phase clouds significantly decreased at rates of 2.06 μm, 2.96 L^{-1}, and 18.54 g m^{-2}, respectively. The IER and LWP of mixed-phase clouds also decreased at rates of 1.95 μm and 111.11 g m^{-2}, respectively. This trend corresponds to the decrease in CT and CF for mixed-phase clouds, and the decrease in CT for ice-phase clouds, as shown in Figure 4, which may be related to the semi-direct effect of aerosols. Huang et al. [78] noted that an increase in atmospheric DU aerosols leads to cloud heating and enhanced cloud droplet evaporation due to the semi-direct effect of aerosols, consequently reducing the cloud water path (CWP). As illustrated in Figure 6c,f, the reduction in LWP was more pronounced compared to the IWP. This observation is similar to the findings of Wang et al. [54], who reported that under the influence of DU aerosols, the cloud optical depth in liquid-phase altocumulus clouds decreases more significantly than in ice-phase altocumulus clouds. This might be attributed to the fact that over the Tibetan Plateau, DU aerosols can significantly heat the atmosphere, with the maximum radiative heating occurring near the ground surface and diminishing with altitude [84]. Compared to ice particles, droplets are more substantially affected by the semi-direct effect of aerosols.

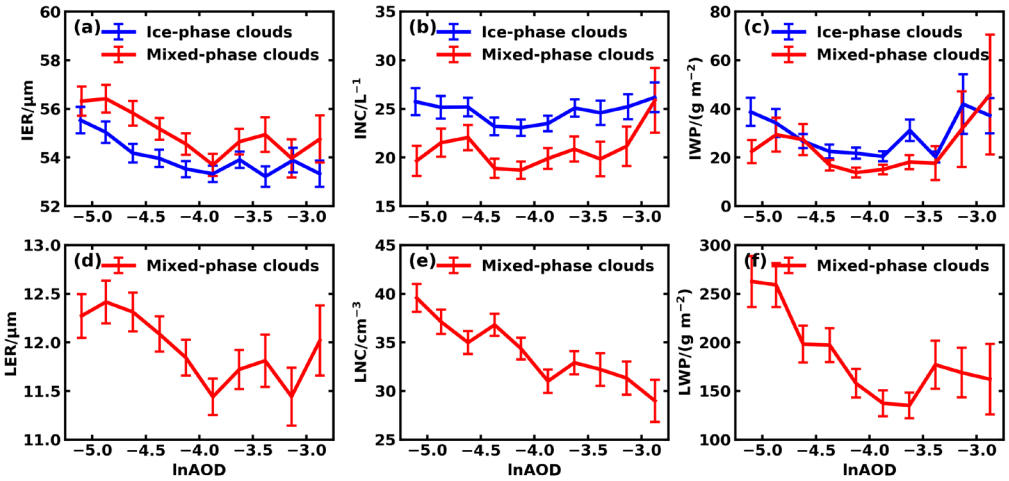

Figure 6. Trends of microphysical characteristics of single-layer non-precipitating ice-phase and mixed-phase clouds over the Tibetan Plateau during the nighttime in MAM and JJA within different logarithmic aerosol optical depth (lnAOD) intervals with changing lnAOD based on CloudSat and CALIPSO data: (**a**) ice particle effective radius (IER), (**b**) ice particle number concentration (INC), (**c**) ice water path (IWP), (**d**) liquid droplet effective radius (LER), (**e**) liquid droplet number concentration (LNC), and (**f**) liquid water path (LWP). The error was calculated as $\frac{s}{\sqrt{n-2}}$, where n is the number of samples for each macrophysical characteristic within each lnAOD interval, and s is the standard deviation.

In the high AOD range, both ice-phase and mixed-phase clouds exhibited an increase in INC and IWP with increasing AOD, while the LNC in mixed-phase clouds tended to decrease, with other physical quantities fluctuating between an increase and a decrease. According to Table S6, the INC of ice-phase clouds and the IWP of mixed-phase clouds significantly increased at rates of 2.22 L^{-1} and 30.39 g m^{-2} per unit change in lnAOD, respectively. The trends in other cloud microphysical characteristics were not significant. The increased INC in ice-phase clouds may have resulted from an increase in the number of aerosols serving as ice nuclei as the AOD increased. This corresponds to the increase in CF of ice-phase clouds shown in Figure 4d. The significant increase in the IWP of mixed-phase clouds with increasing AOD may be related to an enhanced ice formation process within the clouds. Figure 6b,e indicate that within the high AOD range, the INC in mixed-phase clouds increased while the liquid number concentration (LNC) decreased. This could be due to the increase in aerosols promoting the Wegener–Bergeron–Findeisen (WBF) process. Numerical simulations show that DU aerosols, acting as ice nuclei, mainly affect mixed-phase clouds through the WBF process by increasing the INC and reducing the LNC. The presence of DU aerosols leads to a more pronounced WBF process and riming within clouds [85,86].

During SON and DJF nights, the microphysical characteristics of single-layer non-precipitating ice-phase and mixed-phase clouds changed with the AOD as shown in Figure 7. Within the low AOD range (lnAOD ≤ -4.0), as the AOD increased the IER, INC, and IWP of both ice-phase and mixed-phase clouds fluctuated between increasing and decreasing, while the LER, LNC, and LWP of mixed-phase clouds all decreased. According to Table S7, for each unit change in lnAOD, the LNC and LWP of mixed-phase clouds decreased at rates of 4.87 cm^{-3} and 59.30 g m^{-2}, respectively, which may be related to the semi-direct effect of aerosols. Within the high AOD range (lnAOD > -4.0), as the AOD increased, the IER, INC, and IWP of ice-phase clouds generally showed an increasing trend, but only IWP exhibited a significant increasing trend, with an increase rate of 15.40 g m^{-2} per unit lnAOD. The changes in the microphysical characteristics of mixed-phase clouds were minimal.

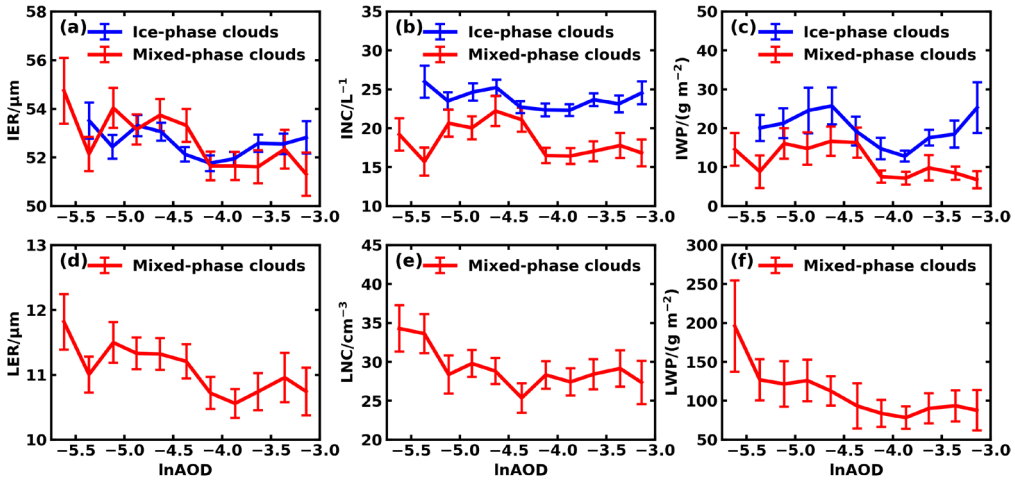

Figure 7. Trends of microphysical characteristics of single-layer non-precipitating ice-phase and mixed-phase clouds over the Tibetan Plateau during the nighttime in SON and DJF within different logarithmic aerosol optical depth (lnAOD) intervals with changing lnAOD based on CloudSat and CALIPSO data: (**a**) ice particle effective radius (IER), (**b**) ice particle number concentration (INC), (**c**) ice water path (IWP), (**d**) liquid droplet effective radius (LER), (**e**) liquid droplet number concentration (LNC), and (**f**) liquid water path (LWP). The error was calculated as $\frac{s}{\sqrt{n-2}}$, where n is the number of samples for each macrophysical characteristic within each lnAOD interval, and s is the standard deviation.

3.3. Correlation between Aerosols and Clouds under Controlled Meteorological Conditions

Although Section 3.2 demonstrates significant correlations and linear relationships between aerosols and some cloud characteristics, numerous meteorological factors can influence both cloud formation and development, as well as aerosol content and correlation between aerosols and cloud characteristics [87–90]. In the following analysis, the PWV, CAPE, and PVV near the cloud base were employed to represent atmospheric moisture and thermodynamic and dynamic conditions [21], respectively. The correlations of these three physical quantities with the AOD were analyzed. During MAM and JJA (SON and DJF) nights, the average CBH of ice-phase clouds was 7.49 (6.81) km, and for mixed-phase clouds it was 6.05 (5.63) km. The atmospheric pressure near the average CBH of ice-phase clouds corresponded to 400 (450) hPa, and for mixed-phase clouds it corresponded to 500 hPa.

For ice-phase and mixed-phase clouds, an increase in the AOD corresponded to trends in the PWV, CAPE, and PVV near the cloud base. These trends align with changes in the macrophysical and microphysical characteristics of the clouds, displaying different patterns on either side of lnAOD = −4.0. In the low AOD range, except for the insignificant trend in PVV near the average cloud base of mixed-phase clouds, the PWV and CAPE corresponding to both ice-phase and mixed-phase clouds exhibited a significant decreasing trend, while the PVV demonstrated a significant increasing trend (as shown in Figure 8 and Table S8). This indicates that with an increase in aerosol content, the atmospheric moisture content decreases, and both the instability energy and upward motion weaken, all changes that are unfavorable for cloud formation and development. In the high AOD range, the PWV, CAPE, and W showed fluctuations between increasing and decreasing trends, without any significant overall trend. In SON and DJF, the PWV and CAPE also showed similar trends of variation with an increasing AOD, while the change in the PVV at 450 (500) hPa with an increasing AOD was minimal (as shown in Figure 9).

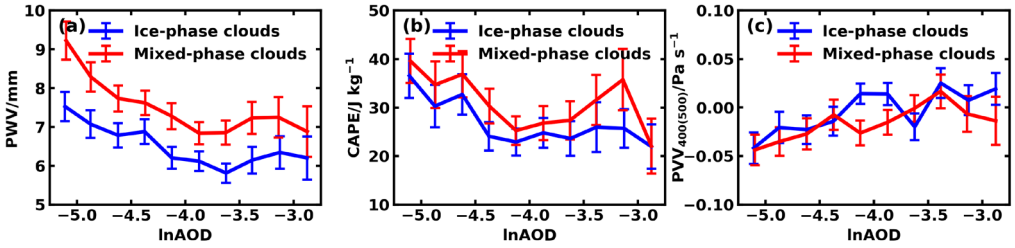

Figure 8. Trends of meteorologic conditions for single-layer non-precipitating ice-phase and mixed-phase clouds over the Tibetan Plateau during the nighttime in MAM and JJA within different logarithmic aerosol optical depth (lnAOD) intervals with changing lnAOD based on ERA5 and CALIPSO data: (**a**) precipitable water vapor (PWV), (**b**) convective available potential energy (CAPE), (**c**) pressure vertical velocity (PVV) at 400 (500) hPa for ice-phase (mixed-phase) clouds ($W_{400(500)}$). The error was calculated as $\frac{s}{\sqrt{n-2}}$, where n is the number of samples for each macrophysical characteristic within each lnAOD interval and s is the standard deviation.

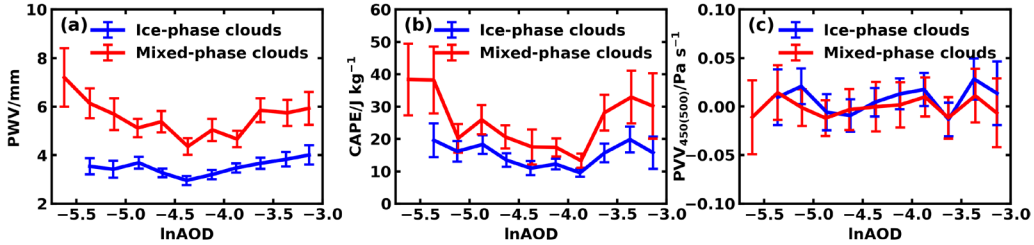

Figure 9. Trends of meteorologic conditions for single-layer non-precipitating ice-phase and mixed-phase clouds over the Tibetan Plateau during the nighttime in SON and DJF within different logarithmic aerosol optical depth (lnAOD) intervals with changing lnAOD based on ERA5 and CALIPSO data: (**a**) precipitable water vapor (PWV), (**b**) convective available potential energy (CAPE), (**c**) pressure vertical velocity (PVV) at 400 (500) hPa for ice-phase (mixed-phase) clouds ($W_{400(500)}$). The error was calculated as $\frac{s}{\sqrt{n-2}}$, where n is the number of samples for each macrophysical characteristic within each lnAOD interval and s is the standard deviation.

Thus, the trends in the macrophysical and microphysical characteristics of clouds with AOD may also be affected by changes in meteorological factors. To eliminate the influence of meteorological factors, the subsequent sections calculate the total and partial correlation coefficients between the low and high range AOD and cloud characteristics, controlling for meteorological factors that may affect the aerosol–cloud correlation.

3.3.1. Macrophysical Characteristics of Clouds

For MAM and JJA nighttime ice-phase and mixed-phase clouds, all data within the ranges of (−5.25, −4.0] and (−4.0, −2.75] not averaged by categorization were taken as the low and high AOD ranges, respectively. The total and partial correlation coefficients between various cloud macrophysical/microphysical characteristics and the lnAOD were calculated. During MAM and JJA nights, the average CTH and CBH of ice-phase clouds were 8.95 km and 7.49 km, respectively, while for mixed-phase clouds they were 7.33 km and 6.05 km, respectively. The atmospheric pressures near the average CTH, within the cloud, and at the CBH for ice-phase clouds corresponded to 250, 350, and 400 hPa, respectively, and for mixed-phase clouds they corresponded to 350, 400, and 500 hPa, respectively.

When the total correlation coefficient between the macrophysical/microphysical characteristics of clouds and the lnAOD was significant, controlling for a certain meteorological factor or all meteorological factor parameters, and calculating the absolute difference between the partial correlation coefficient and the total correlation coefficient, the meteorological factors are sorted from top to bottom according to the absolute magnitude of the difference in Tables S10–S13.

Figure 10 shows that for MAM and JJA in the nighttime, single-layer non-precipitating ice-phase and mixed-phase clouds within the low and high AOD ranges, the total correlation coefficients between the AOD and the macrophysical characteristics of clouds (the first column in figure), and the partial correlation coefficients between AOD and the macrophysical characteristics of clouds, both when controlling for various single meteorological factors (columns 2–19 in figure) and when controlling for all meteorological factors simultaneously (column 20 in figure). In the low AOD range, the total correlation coefficient between the CBH of ice-phase clouds and the lnAOD was significant. After removing the influence of 18 meteorological factors, the partial correlation coefficients exhibited varying levels of significance. Specifically, the partial correlation coefficients were not significant when controlling for factors such as CAPE, the RH near the average cloud top and cloud base heights, the V near the average CTH, the PVV near the average CBH, and when controlling for all 18 meteorological factors simultaneously. This indicates that the CBH of ice-phase clouds is influenced not only by aerosols but also by meteorological conditions, particularly CAPE, RH, and horizontal wind speed near the cloud top; and RH and PVV near the cloud base. For the CT of ice-phase clouds, both total and partial correlation coefficients consistently showed a significant negative correlation, indicating that meteorological factors have a minor impact on the CT of ice-phase clouds compared to aerosols. The significant negative correlation coefficient indicates that an increase in aerosols may lead to a decrease in the CT of ice-phase clouds. Similarly, it can be deduced that for mixed-phase clouds, the CTH and CF are affected by both aerosols and meteorological conditions. The T near the cloud top, within the cloud, and near the cloud base has a prominent impact on the CTH, while PWV and T near the cloud top and within the cloud significantly affect the CF. The reduction in the CT of mixed-phase clouds is likely primarily affected by aerosols.

In the high AOD range, there was a strong correlation between aerosols and the macrophysical characteristics of ice-phase clouds, while the correlation with mixed-phase clouds was very weak. Aerosols have a significant impact on the CTH and CBH of ice-phase clouds; an increase in aerosols may lead to higher cloud top and base heights. The CT and CF are influenced both by aerosols and meteorological conditions. The RH near the cloud top and within the cloud significantly affects the CT and CF. Additionally, the T near the cloud top, within the cloud, and near the cloud base also significantly impacts the CF.

For SON and DJF nighttime ice-phase (mixed-phase) clouds, all data within the ranges of $(-5.5, -4.0]$ and $(-4.0, -3.0]$ ($(-5.75, -4.0]$ and $(-4.0, -3.0]$) not averaged by categorization were taken as the low and high AOD ranges, respectively, to calculate the total and partial correlation coefficients between various cloud macrophysical and microphysical characteristics and the lnAOD. During SON and DJF nights, the average CTH and CBH for ice-phase clouds were 8.06 km and 6.81 km, respectively, and for mixed-phase clouds they were 6.60 km and 5.63 km, respectively. The atmospheric pressures near the average cloud top, within the cloud, and at the cloud base for ice-phase clouds corresponded to 350, 400, and 450 hPa, respectively, and for mixed-phase clouds they corresponded to 400, 450, and 500 hPa, respectively.

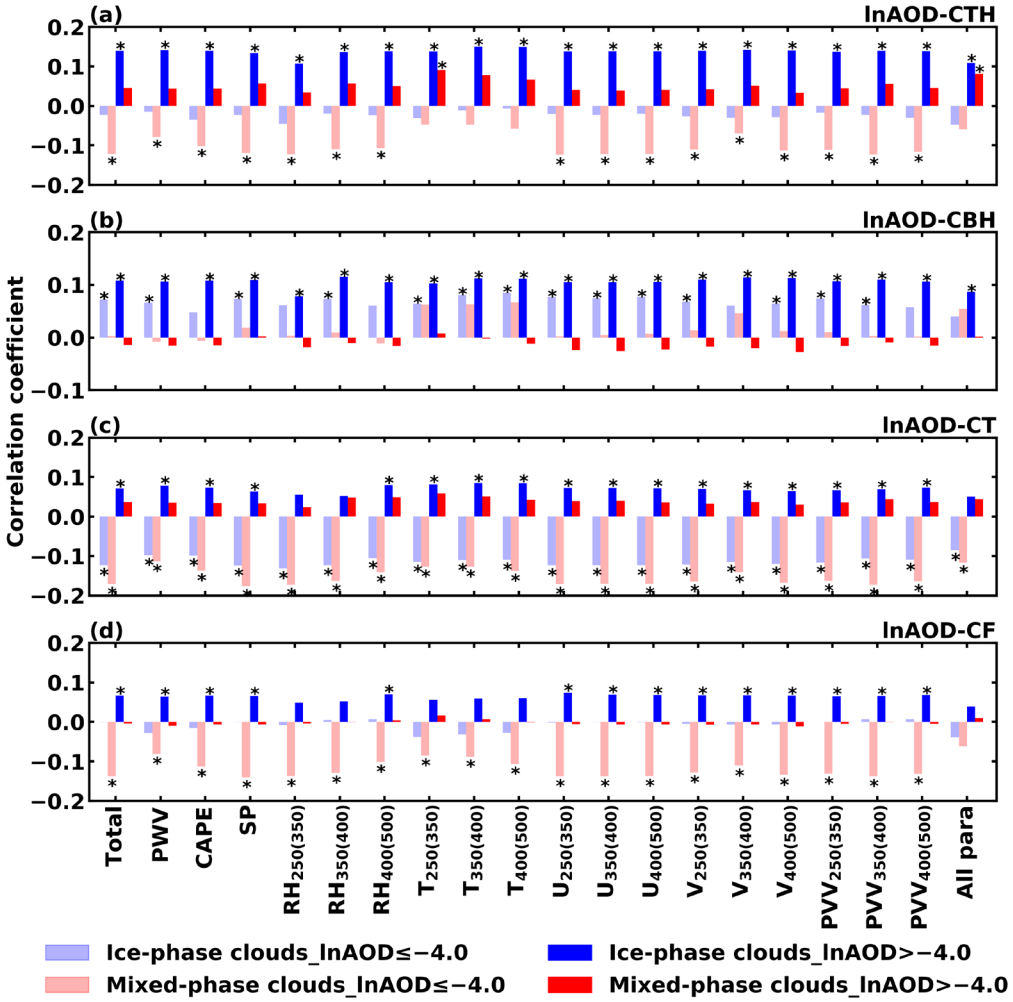

Figure 10. During the nighttime in MAM and JJA over the Tibetan Plateau, for single-layer non-precipitating ice-phase and mixed-phase clouds under the conditions of logarithmic aerosol optical depth (lnAOD) ≤ -4.0 and lnAOD > -4.0, the total correlation coefficients (column 1) between lnAOD and various macrophysical characteristics of clouds: (**a**) cloud top height (CTH), (**b**) cloud base height (CBH), (**c**) cloud thickness (CT), (**d**) cloud fraction (CF), and the partial correlation coefficients after individually (column 2–19) and simultaneously (column 20) removing the influence of 18 meteorological factors (the values in parentheses correspond to the mixed-phase clouds at specific pressures) based on CloudSat, CALIPSO, and ERA5 data, with * indicating passing the 95% significance test.

During SON and DJF nights (as shown in Figure 11), within the low AOD range, the total and partial correlation coefficients between the macrophysical characteristics of ice-phase clouds and the lnAOD were not significant. The total correlation coefficients of the CTH, CT, and CF for mixed-phase clouds with the lnAOD were negatively correlated and significant, but not all partial correlation coefficients were significant. The CTH, CT, and CF are likely influenced by both aerosols and meteorological conditions, with PWV, CAPE, SP, and T near the cloud top, within the cloud, and at the cloud base, and horizontal wind speed having a notable impact on the CTH, and PWV, CAPE, and temperatures near the cloud top, within the cloud, and at the cloud base significantly affecting the CT and CF. Within the high AOD range, the total and partial correlation coefficients between the macrophysical characteristics of both ice-phase and mixed-phase clouds and lnAOD were not significant.

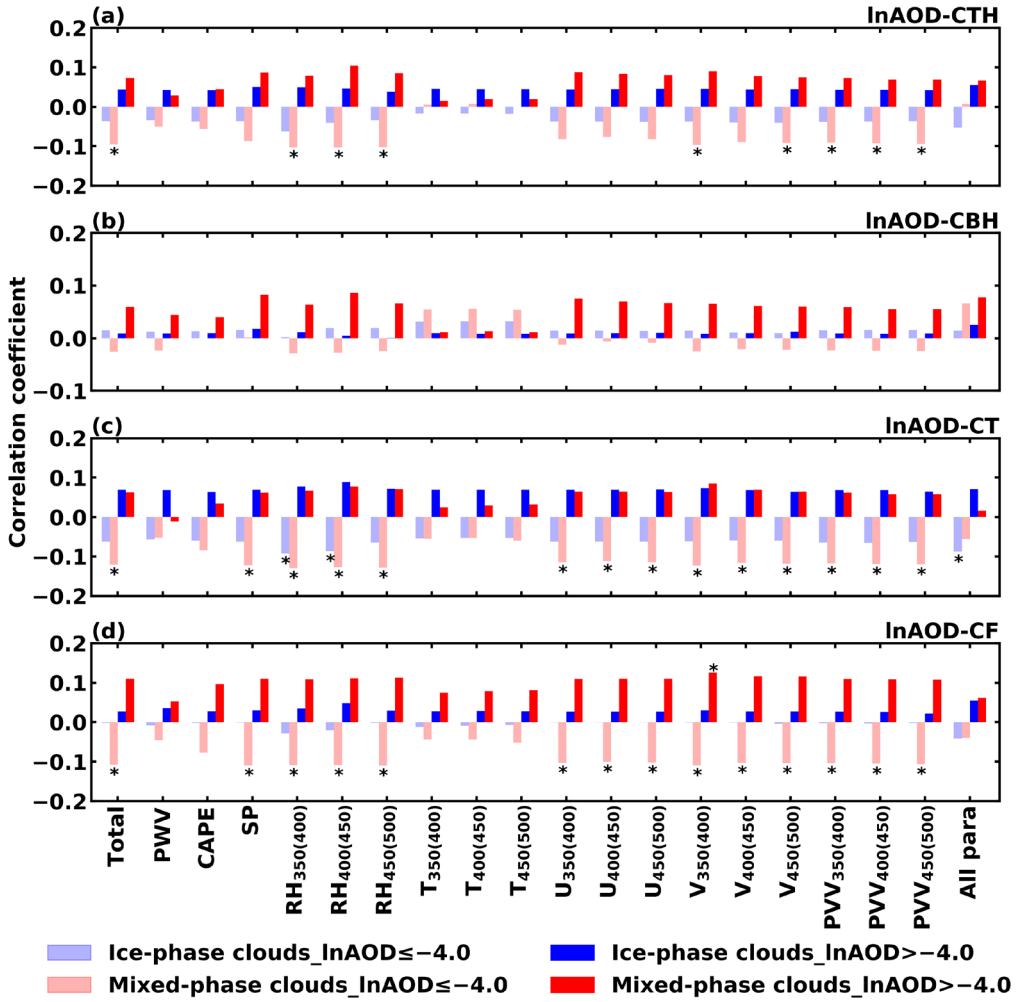

Figure 11. During the nighttime in SON and DJF over the Tibetan Plateau, for single-layer non-precipitating ice-phase and mixed-phase clouds under the conditions of logarithmic aerosol optical depth (lnAOD) ≤ -4.0 and lnAOD > -4.0, the total correlation coefficients (column 1) between lnAOD and various macrophysical characteristics of clouds: (**a**) cloud top height (CTH), (**b**) cloud base height (CBH), (**c**) cloud thickness (CT), (**d**) cloud fraction (CF), and the partial correlation coefficients after individually (column 2–19) and simultaneously (column 20) removing the influence of 18 meteorological factors (the values in parentheses correspond to the mixed-phase clouds at specific pressures) based on CloudSat, CALIPSO, and ERA5 data, with * indicating passing the 95% significance test.

3.3.2. Microphysical Characteristics of Clouds

During MAM and JJA nights, the correlation coefficients between lnAOD and various cloud microphysical characteristics are shown in Figure 12. In the low AOD range, an increase in aerosol content may lead to a reduction in both the IER and IWP of ice-phase clouds. The INC is greatly affected by meteorological conditions, especially by the CAPE and RH near the cloud base, and the PVV near the cloud top, within the cloud, and near the cloud base. In mixed-phase clouds, the IER, IWP, LER, and LNC are influenced by both aerosols and meteorological conditions. Specifically, the IER and IWP are greatly affected by PWV. Meanwhile, the LER and LNC are significantly influenced by PWV, CAPE, and T near the cloud top, within the cloud, and near the cloud base. The LWP in mixed-phase clouds is primarily influenced by aerosols, with a higher aerosol content resulting in a lower LWP value. In the high AOD range, the total and partial correlation coefficients between aerosols and various microphysical quantities were not significant.

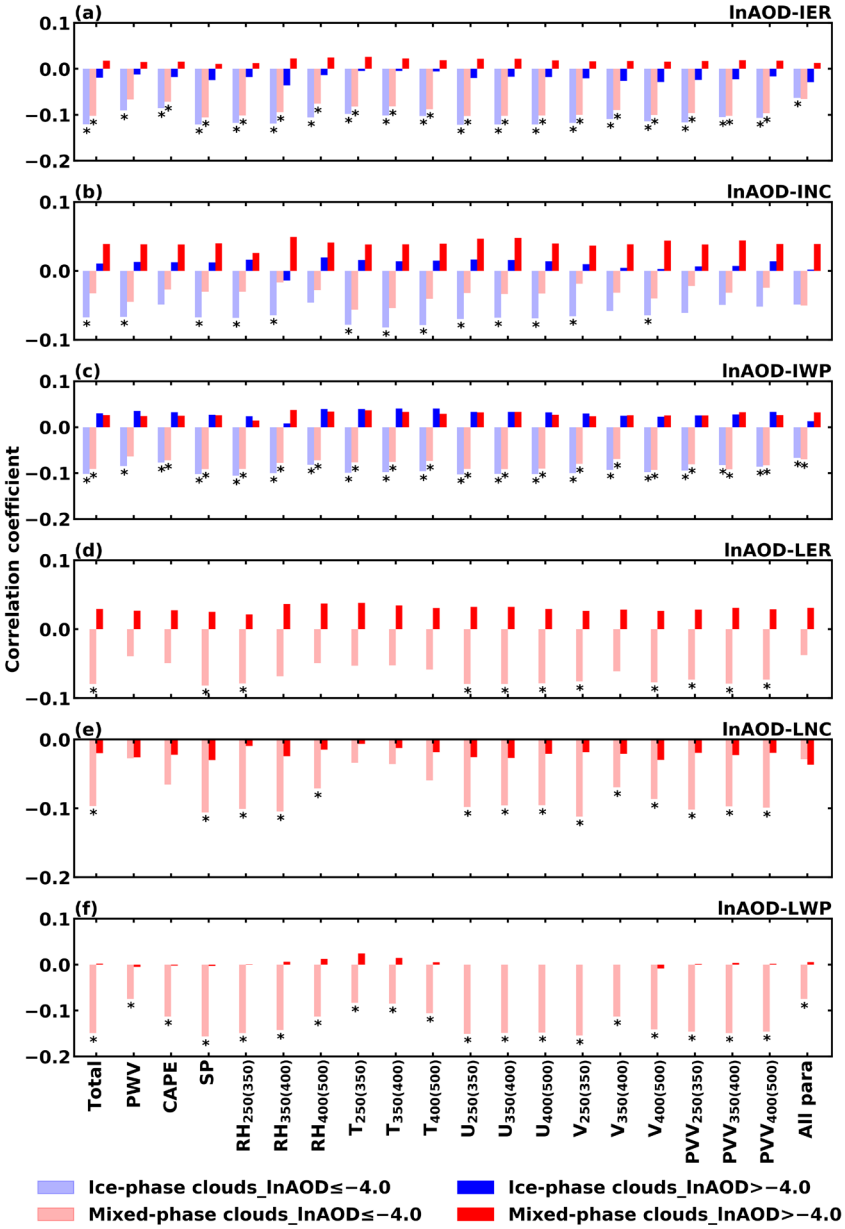

Figure 12. During the nighttime in MAM and JJA over the Tibetan Plateau, for single-layer non-precipitating ice-phase and mixed-phase clouds under the conditions of logarithmic aerosol optical depth (lnAOD) ≤ -4.0 and lnAOD > -4.0, the total correlation coefficients (column 1) between lnAOD and various microphysical characteristics of clouds: (**a**) ice particle effective radius (IER), (**b**) ice particle number concentration (INC), (**c**) ice water path (IWP), (**d**) liquid droplet effective radius (LER), (**e**) liquid droplet number concentration (LNC), (**f**) liquid water path (LWP), and the partial correlation coefficients after individually (column 2–19) and simultaneously (column 20) removing the influence of 18 meteorological factors (the values in parentheses correspond to the mixed-phase clouds at specific pressures) based on CloudSat, CALIPSO, and ERA5 data, with * indicating passing the 95% significance test.

During SON and DJF nights, the correlation coefficients between lnAOD and various cloud microphysical characteristics are shown in Figure 13. Within the low AOD range, the IER of ice-phase clouds and the IER, LER, LNC, and LWP of mixed-phase clouds may all be influenced by both aerosols and meteorological conditions. The IER of ice-phase clouds and the LER of mixed-phase clouds are significantly affected by PWV, and the T near the cloud top, within the cloud, and near the cloud base. The IER of mixed-phase

clouds is also affected by CAPE and the PVV near the cloud base; LNC is additionally influenced by CAPE. LWP is primarily affected by the T near the cloud top and within the cloud. Within the high AOD range, the total correlation coefficients between aerosols and various microphysical characteristics did not reach a level of significance, indicating a complex relationship between aerosols and cloud microphysical characteristics under these conditions. This complexity may be related to the combined effects of changes in cloud macrophysical characteristics, aerosol influences, meteorological conditions, etc.

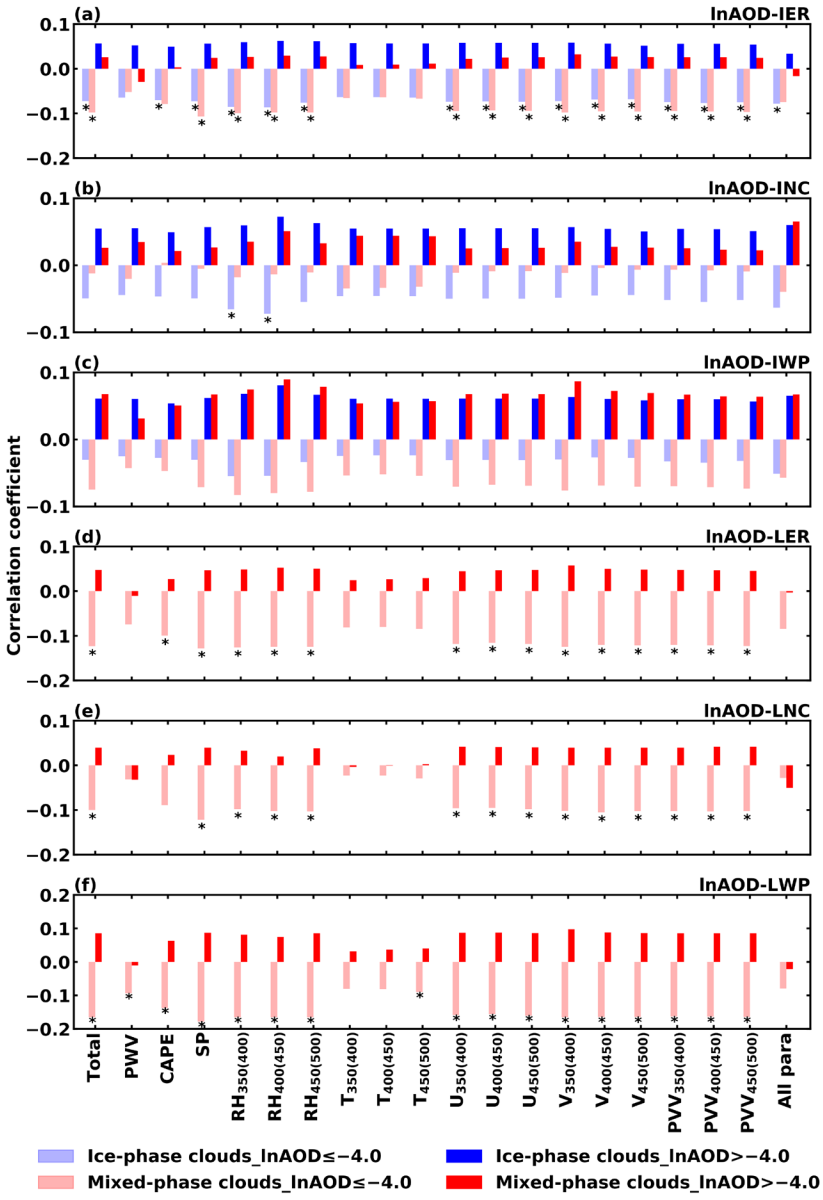

Figure 13. During the nighttime in SON and DJF over the Tibetan Plateau, for single-layer non-precipitating ice-phase and mixed-phase clouds under the conditions of logarithmic aerosol optical depth (lnAOD) ≤ -4.0 and lnAOD > -4.0, the total correlation coefficients (column 1) between lnAOD and various microphysical characteristics of clouds: (**a**) ice particle effective radius (IER), (**b**) ice particle number concentration (INC), (**c**) ice water path (IWP), (**d**) liquid droplet effective radius (LER), (**e**) liquid droplet number concentration (LNC), (**f**) liquid water path (LWP), and the partial correlation coefficients after individually (column 2–19) and simultaneously (column 20) removing the influence of 18 meteorological factors (the values in parentheses correspond to the mixed-phase clouds at specific pressures) based on CloudSat, CALIPSO, and ERA5 data, with * indicating passing the 95% significance test.

4. Discussion

4.1. The Potential Effects of Aerosols on Clouds

According to the MERRA-2 reanalysis data, the proportion of DU aerosols is relatively high in MAM and JJA, while SU aerosols are highest in SON and DJF. Therefore, the correlation between aerosols and ice-phase and mixed-phase clouds was analyzed for MAM and JJA, and SON and DJF separately. The results indicated that during MAM and JJA nights, the influence of aerosols on ice-phase and mixed-phase clouds may be more significant than during SON and DJF nights. This suggests that for clouds containing ice-phase processes, the impact of DU aerosols on clouds may be more significant than that of SU aerosols.

During MAM and JJA nights, in the low range of AOD values, aerosols may inhibit the vertical development of ice-phase and mixed-phase clouds, resulting in a decrease in the CT and CWP, and the semi-direct effect of aerosols may play a dominant role. Wang et al. [91] also found in their observational study of aerosols in the Lhasa region that although the aerosol load is low over the Tibetan Plateau, the heating effect of aerosols due to strong solar radiation absorption is significant for warming the Earth-atmosphere system. In the high range of AOD values, aerosols may promote the vertical development of ice-phase clouds, leading to an increase in the CTH and the CBH, and the indirect effect and activation effect of aerosols may play a dominant role. This is similar to the findings of Jiang et al. [7] on deep convective clouds in Southeast Asia, where DU aerosols at lower AOD levels hindered cloud development but tended to facilitate it at higher levels. This nonlinear impact of aerosols on clouds might relate to the aerosol layer's position. Yin and Chen [92] discovered through numerical simulations that when the temperature of the dust layer is above -5 °C, the heating effect of DU aerosols prevents cloud droplet formation and reduces the cloud optical thickness. In contrast, below -5 °C, DU aerosols serve as effective ice nuclei, enhancing the formation of ice crystals and promoting the development of clouds and precipitation. The results of the partial correlation analysis in this study also indicated that temperature has a significant influence on the correlation between aerosols and clouds.

Many numerical simulation studies have shown that the relative contributions of aerosols' direct, semi-direct, and indirect effects on ACIs are different. For instance, some researchers have found that aerosols in urban areas primarily affect clouds and precipitation through indirect effects [93–95], but Fan et al. [96] found in a heavy rainfall event in the Sichuan Basin that aerosols mainly exerted a radiative effect on clouds and precipitation, with minimal indirect effects. Ackerman et al. [97] found that aerosols during the northeast monsoon over the Indian Ocean are dominated by semi-direct effects. These discrepancies may be due to various factors such as the temporal and spatial simulation scales, the average CF during the simulation period, the type of aerosols, and their vertical distribution, etc. [98,99]. A previous study by Liu et al. [57] over the Tibetan Plateau showed that aerosols may increase the IWP of ice-phase clouds at nighttime, suggesting that the impact of aerosols on ice-phase clouds may be primarily through microphysical effects. However, the results of this study indicate that, during MAM and JJA nights over the Tibetan Plateau when the AOD is low, the impact of aerosols on ice-phase clouds may be primarily through semi-direct effects. When the AOD is high, the impact of aerosols on ice-phase clouds may be primarily through microphysical effects. The different conclusions obtained in this study under low AOD conditions may be related to the exclusion of multi-layer clouds and precipitation clouds. Additionally, this may also be related to the higher temporal resolution of the data used in this study. Since aerosol semi-direct effects can rapidly adjust the atmospheric temperature structure and change the distribution of clouds [100], at longer time and broader spatial scales, aerosol semi-direct effects may be more easily averaged out [98].

4.2. Preliminary Quantification of the Interactions of Aerosols and Clouds

In the atmosphere, aerosol particles can act as cloud condensation nuclei or ice nuclei, so an increase in aerosol content often implies an increase in cloud condensation nuclei or ice nuclei. For liquid-phase clouds, when the LWP in the cloud is constant, an increase in the LNC will result in a decrease in the LER and an increase in the cloud optical depth. This mechanism is referred to as the "Twomey effect" or the first indirect aerosol effect [35]. Feingold et al. [101] pointed out that the aerosol first indirect effect's ACI can be calculated using the following formula:

$$\mathrm{ACI} = -\frac{\partial \ln r_e}{\partial \ln \alpha}|_{\mathrm{CWP}}, \quad (4)$$

where r_e represents the cloud droplet effective radius, α represents the aerosol concentration, CWP represents the cloud water path, and a positive ACI value indicates that r_e decreases with an increasing α.

Many scholars have studied the interaction between aerosols and liquid-phase clouds using ACI values [12,19,20,22,23], and some scholars have investigated the interaction between aerosols and ice-phase clouds using ACI values [102]. Due to the nonlinear and multi-scale nature of ACIs, as well as the incomplete understanding of the relevant physical processes, quantifying ACIs is very challenging [103]. This study attempted to preliminarily quantify the interaction between aerosols and ice-phase and mixed-phase clouds over the Tibetan Plateau using CloudSat/CALIPSO satellite data. For ice-phase and mixed-phase clouds, α was the AOD calculated from CALIPSO data. For ice-phase clouds, r_e represents the IER, and CWP represents the IWP; for mixed-phase clouds, r_e is taken as both the IER and the LER, and CWP is the sum of the LWP and the IWP.

During MAM and JJA nights, and SON and DJF nights, the ACI values calculated based on IER/LER for ice-phase clouds in different IWP ranges and mixed-phase clouds in different CWP ranges (the distribution histograms of IWP for ice-phase clouds and CWP for mixed-phase clouds are shown in Figures S3 and S4, respectively) are presented in Table 2. It can be seen from the table that during MAM and JJA nights, when the IWP of ice-phase clouds was in the range of 1–5 g m^{-2} and 5–10 g m^{-2}, the IER was negatively correlated with AOD, with ACI_{IER} values of 0.10×10^{-1} and 0.18×10^{-1}, respectively, and passed the 95% significance test. This result is consistent with the "Twomey effect", which may be due to the higher DU aerosol content in MAM and JJA, as DU aerosols are effective ice nuclei that can promote the formation of ice particles in clouds [79,80,104]. The ACI_{IER} and ACI_{LER} for mixed-phase clouds were not significant in all CWP ranges.

Table 2. During MAM and JJA, and SON and DJF nights, the ACI (aerosol–cloud interaction)$_{IER}$ values based on ice particle effective radius (IER) for single-layer non-precipitating ice-phase clouds in different IWP (ice water path) ranges, and the ACI_{IER}/ACI_{LER} values based on IER/liquid droplet effective radius (LER) for mixed-phase clouds in different CWP (cloud water path) ranges based on CloudSat, and CALIPSO data, with * indicating passing the 95% significance test.

			MAM and JJA		**SON and DJF**	
			ACI_{IER}	**ACI_{LER}**	**ACI_{IER}**	**ACI_{LER}**
Ice-phase clouds	IWP/(g m^{-2})	1–5	0.10×10^{-1} *		0.06×10^{-1}	
		5–10	0.18×10^{-1} *		0.03×10^{-1}	
		10–15	0.14×10^{-1}		-0.03×10^{-1}	
Mixed-phase clouds	CWP/(g m^{-2})	10–50	-0.46×10^{-2}	-0.26×10^{-2}	0.49×10^{-2}	0.70×10^{-2}
		50–100	0.69×10^{-2}	-0.02×10^{-2}	1.83×10^{-2}	3.78×10^{-2} *
		100–150	0.41×10^{-2}	-0.84×10^{-2}	0.77×10^{-2}	-0.01×10^{-2}
		150–200	-1.29×10^{-2}	-1.69×10^{-2}	-4.31×10^{-2}	-0.06

During SON and DJF nights, the absolute values of ACI for ice-phase clouds were lower than those during MAM and JJA, and they were not significant. This indicates that the aerosol first indirect effect in ice-phase clouds during SON and DJF is weaker than

that during MAM and JJA, which may be related to the decrease in DU during SON and DJF, leading to a decrease in ice nuclei. For mixed-phase clouds, when the CWP was between 50 and 100 g m^{-2}, the ACI_{LER} was 3.78 × 10^{-2}, and the LER was significantly negatively correlated with the AOD, consistent with the "Twomey effect". This may be because during SON and DJF, the aerosols are mainly composed of SU, and SU aerosols have strong hygroscopicity, making them effective cloud condensation nuclei [82,83]. With an increasing AOD, more activated cloud droplets compete for water vapor under limited water vapor conditions, leading to a decrease in the LER.

During MAM and JJA nights, the ACI of ice-phase clouds was positive; during SON and DJF nights, the ACI values of ice-phase clouds were lower than those in MAM and JJA. This result is similar to the results of Patel and Kumar [102] in northern India, but the absolute values of ACI were much lower than their calculated values. Due to the limited research on ACI calculation in mixed-phase clouds, this study compared the results with ACI values obtained in liquid-phase clouds and found that they were much lower than those of the previous study [12,20,22,23]. This may be related to the different time scales of the data analysis. Previous studies mostly used monthly averaged data, while this study used polar satellite orbit data, which has a smaller time scale. Li et al. [103] used machine learning and observational data to show that ACI has stronger randomness at shorter time scales and smaller sampling areas. The stronger randomness may prevent the aerosol's first indirect effect from manifesting in all samples, resulting in small ACI values when considering different samples from many different time points and limited sampling areas. Additionally, it may be because aerosols in plateau regions have a strong solar radiation absorption capability, leading to strong heating effects [91], which enhances the semi-direct effect of aerosols and weakens the aerosol's first indirect effect. Furthermore, it may be because, at smaller time scales and limited spatial scales, compared to aerosols, clouds are more influenced by meteorological factors, resulting in small ACI values.

5. Conclusions

Using CloudSat/CALIPSO satellite data from 2006 to 2010, along with MERRA-2 and ERA5 reanalysis data, this study examined the spatial distribution characteristics of aerosols and clouds over the Tibetan Plateau region across all seasons. It further investigated how nighttime aerosols during the MAM and JJA seasons, as well as the SON and DJF seasons, influence the macrophysical and microphysical characteristics of single-layer non-precipitating ice-phase and mixed-phase clouds, and preliminarily quantified the interactions of aerosols and ice-phase and mixed-phase clouds. The main conclusions are as follows:

(1) Based on MERRA-2 reanalysis data, the aerosol optical depth (AOD) over the Tibetan Plateau was higher in MAM and JJA than in SON and DJF, with aerosols primarily composed of dust, sulfate, and organic carbon. The cloud phases are predominantly ice-phase and mixed-phase. During MAM and JJA, dust aerosols accounted for a higher proportion, representing over 40% of the total AOD, while during SON and DJF, sulfate aerosols significantly outweighed other types of aerosols, accounting for 54% and 47%, respectively. According to CloudSat satellite data, in each season, the cloud fraction of ice-phase clouds was the highest, followed by mixed-phase and liquid-phase.

(2) Based on CloudSat/CALIPSO satellite data and ERA5 reanalysis data, the macrophysical and microphysical characteristics of ice-phase and mixed-phase clouds exhibited non-linear changes with an increasing AOD. When the lnAOD was ≤ -4.0, with an increasing AOD during MAM and JJA nights, for every unit change in the lnAOD, the cloud thickness and ice particle effective radius of ice-phase clouds (mixed-phase clouds) decreased at speeds of 0.41 km (0.47 km) and 2.06 μm (1.95 μm), respectively, while the ice water path of ice-phase clouds and the liquid water path of mixed-phase clouds decreased at speeds of 18.54 g m^{-2} and 111.11 g m^{-2}, respectively. The ice particle number concentration of ice-phase clouds and the cloud fraction of mixed-phase

clouds also decreased at speeds of 2.96 L^{-1} and 7.05%, respectively. During SON and DJF nights, for every unit change in lnAOD, the cloud thickness of ice-phase clouds, the cloud top height of mixed-phase clouds, the liquid droplet number concentration, and the liquid water path decreased at speeds of 0.19 km, 0.34 km, 4.87 cm^{-3}, and 59.30 g m^{-2}, respectively. When the lnAOD was >-4.0, with an increasing AOD during MAM and JJA nights, for every unit change in the lnAOD, the cloud top height, cloud base height, cloud fraction, ice particle number concentration of ice-phase clouds, and the ice water path of mixed-phase clouds increased at speeds of 0.61 km, 0.31 km, 7.9%, 2.22 L^{-1}, and 30.39 g m^{-2}, respectively. During MAM and DJF nights, for every unit change in the lnAOD, the cloud fraction of mixed-phase clouds and the ice water path of ice-phase clouds increased at speeds of 7.88% and 15.40 g m^{-2}, respectively.

(3) Based on CloudSat/CALIPSO satellite data and ERA5 data, after a partial correlation analysis excluding the influence of meteorological factors on the correlation between aerosols and clouds, during MAM and JJA nights, when the lnAOD is ≤ -4.0, an increase in aerosols may lead to thinning of ice-phase and mixed-phase cloud layers and a decrease in cloud water path values; when the lnAOD is >-4.0, an increase in aerosols may cause the cloud base and cloud top heights of ice-phase clouds to rise. During SON and DJF nights, changes in the macrophysical and microphysical characteristics of ice-phase and mixed-phase clouds may be influenced by both meteorological factors and aerosols.

(4) Based on CloudSat/CALIPSO satellite data, during MAM and JJA nights, when the ice water path of ice-phase clouds was in the range of 1–5 g m^{-2} and 5–10 g m^{-2}, the ice particle effective radius was negatively correlated with the AOD. The ACI values were 0.10×10^{-1} and 0.18×10^{-1}, respectively, and passed the 95% significance test, consistent with the "Twomey effect" phenomenon.

This paper primarily utilized satellite data to analyze how aerosols affect the macrophysical and microphysical characteristics of ice-phase and mixed-phase clouds over the Tibetan Plateau. However, the results still exhibited significant uncertainty, and the understanding of the mechanisms governing the interaction between aerosols and clouds of different phases remains unclear. Future research should combine numerical models, comprehensive observations, and other methods to further investigate and elucidate the interaction mechanisms between different types of aerosols and clouds of different phases over the plateau.

Supplementary Materials: The following supporting information can be downloaded at: https://www.mdpi.com/article/10.3390/rs16101781/s1, Figures S1–S4; Tables S1–S13.

Author Contributions: Conceptualization, S.Z., Y.Q. and C.L.; methodology, Y.Q., C.L. and J.Y.; software, S.Z. and Y.Q.; validation, S.Z., Y.Q., L.Q., X.M. and C.L.; formal analysis, Y.Q., C.L. and X.M.; investigation, Y.Q., C.L. and X.M.; resources, Y.Q.; data curation, S.Z. and Y.Q.; writing—original draft preparation, S.Z., Y.Q. and X.M.; writing—review and editing, S.Z., L.Q., Y.Q., X.M., J.Y., X.H., J.L., L.Z., J.G. and C.L.; visualization, S.Z. and Y.Q.; supervision, Y.Q. and C.L.; project administration, Y.Q. and C.L.; funding acquisition, Y.Q., X.M. and C.L. All authors have read and agreed to the published version of the manuscript.

Funding: This work was supported by the Second Tibetan Plateau Scientific Expedition Program (2019QZKK0104), the National Natural Science Foundation of China (42075077, 42165008), the National Key Research and Development Program of China (2019YFC1510302), the Qinghai Provincial Science and Technology Department Project (2021-ZJ-745), the Innovation Team Project of Qinghai Provincial Meteorological Bureau (QXTD2024-02), and the Natural Science Foundation of Gansu Province, China (21JR7RA711).

Data Availability Statement: Publicly available datasets were analyzed in this study. The MERRA-2 data provided by the Global Modeling and Assimilation Office can be downloaded from https://gmao.gsfc.nasa.gov/reanalysis/MERRA-2/ (accessed on 11 January 2023). CALIPSO data can be downloaded from https://subset.larc.nasa.gov/calipso/ (accessed on 19 October 2022). CloudSat

data can be downloaded from https://www.cloudsat.cira.colostate.edu/ (accessed on 8 October 2022). The ERA5 data provided by ECMWF can be downloaded from https://cds.climate.copernicus.eu/cdsapp#!/search?type=dataset (accessed on 1 December 2023).

Acknowledgments: We are grateful to the National Key Scientific and Technological Infrastructure project "Earth System Science Numerical Simulator Facility" (EarthLab) and the High Performance Computing Center of Nanjing University of Information Science and Technology for performing the numerical calculations in this paper on their cluster system.

Conflicts of Interest: The authors declare no conflicts of interest.

References

1. Intergovernmental Panel on Climate Change (IPCC). Climate change 2021: The physical science basis. In *Contribution of Working Group I to the Sixth Assessment Report of the Intergovernmental Panel on Climate Change*; Cambridge University Press: Cambridge, UK; New York, NY, USA, 2023; pp. 923–1054. [CrossRef]
2. Bender, F.A.M.; Frey, L.; McCoy, D.T.; Grosvenor, D.P.; Mohrmann, J.K. Assessment of aerosol-cloud-radiation correlations in satellite observations, climate models and reanalysis. *Clim. Dyn.* **2019**, *52*, 4371–4392. [CrossRef]
3. Redemann, J.; Wood, R.; Zuidema, P.; Doherty, S.J.; Luna, B.; LeBlanc, S.E.; Diamond, M.S.; Shinozuka, Y.; Chang, I.Y.; Ueyama, R.; et al. An overview of the ORACLES (ObseRvations of Aerosols above CLouds and their intEractionS) project: Aerosol-cloud-radiation interactions in the southeast Atlantic basin. *Atmos. Chem. Phys.* **2021**, *21*, 1507–1563. [CrossRef]
4. Rosenfeld, D.; Andreae, M.O.; Asmi, A.; Chin, M.; de Leeuw, G.; Donovan, D.P.; Kahn, R.; Kinne, S.; Kivekäs, N.; Kulmala, M.; et al. Global observations of aerosol-cloud-precipitation-climate interactions. *Rev. Geophys.* **2014**, *52*, 750–808. [CrossRef]
5. Zelinka, M.D.; Andrews, T.; Forster, P.M.; Taylor, K.E. Quantifying components of aerosol-cloud-radiation interactions in climate models. *J. Geophys. Res.-Atmos.* **2014**, *119*, 7599–7615. [CrossRef]
6. Sharma, P.; Ganguly, D.; Sharma, A.K.; Kant, S.; Mishra, S. Assessing the Aerosols, Clouds and Their Relationship Over the Northern Bay of Bengal Using a Global Climate Model. *Earth Space Sci.* **2023**, *10*, e2022EA002706. [CrossRef]
7. Jiang, J.H.; Su, H.; Huang, L.; Wang, Y.; Massie, S.; Zhao, B.; Omar, A.; Wang, Z.E. Contrasting effects on deep convective clouds by different types of aerosols. *Nat. Commun.* **2018**, *9*, 3874. [CrossRef] [PubMed]
8. Lu, C.S.; Zhu, L.; Liu, Y.G.; Mei, F.; Fast, J.D.; Pekour, M.S.; Luo, S.; Xu, X.Q.; He, X.; Li, J.J.; et al. Observational study of relationships between entrainment rate, homogeneity of mixing, and cloud droplet relative dispersion. *Atmos. Res.* **2023**, *293*, 106900. [CrossRef]
9. Ma, X.; Jia, H.; Yu, F.; Quaas, J. Opposite Aerosol Index-Cloud Droplet Effective Radius Correlations Over Major Industrial Regions and Their Adjacent Oceans. *Geophys. Res. Lett.* **2018**, *45*, 5771–5778. [CrossRef]
10. Pan, Z.X.; Mao, F.Y.; Wang, W.; Logan, T.; Hong, J. Examining Intrinsic Aerosol-Cloud Interactions in South Asia Through Multiple Satellite Observations. *J. Geophys. Res.-Atmos.* **2018**, *123*, 11210–11224. [CrossRef]
11. Qiu, Y.M.; Zhao, C.F.; Guo, J.P.; Li, J.M. 8-Year ground-based observational analysis about the seasonal variation of the aerosol-cloud droplet effective radius relationship at SGP site. *Atmos. Environ.* **2017**, *164*, 139–146. [CrossRef]
12. Saponaro, G.; Kolmonen, P.; Sogacheva, L.; Rodriguez, E.; Virtanen, T.; de Leeuw, G. Estimates of the aerosol indirect effect over the Baltic Sea region derived from 12 years of MODIS observations. *Atmos. Chem. Phys.* **2017**, *17*, 3133–3143. [CrossRef]
13. Yang, Y.K.; Zhao, C.F.; Wang, Y.; Zhao, X.; Sun, W.X.; Yang, J.; Ma, Z.S.; Fan, H. Multi-Source Data Based Investigation of Aerosol-Cloud Interaction Over the North China Plain and North of the Yangtze Plain. *J. Geophys. Res.-Atmos.* **2021**, *126*, e2021JD035609. [CrossRef]
14. Almeida, G.P. The Role Played by the Bulk Hygroscopicity on the Prediction of the Cloud Condensation Nuclei Concentration Inside the Urban Aerosol Plume in Manaus, Brazil: From Measurements to Modeled Results. *Atmos. Environ.* **2023**, *295*, 119517. [CrossRef]
15. Garrett, T.J.; Zhao, C.F. Increased Arctic cloud longwave emissivity associated with pollution from mid-latitudes. *Nature* **2006**, *440*, 787–789. [CrossRef] [PubMed]
16. Zhao, C.F.; Yang, Y.K.; Fan, H.; Huang, J.P.; Fu, Y.F.; Zhang, X.Y.; Kang, S.C.; Cong, Z.Y.; Letu, H.; Menenti, M. Aerosol characteristics and impacts on weather and climate over the Tibetan Plateau. *Natl. Sci. Rev.* **2020**, *7*, 492. [CrossRef] [PubMed]
17. Liu, Y.; Huang, J.; Wang, T.; Li, J.; Yan, H.; He, Y.J.E.-S.R. Aerosol-cloud interactions over the Tibetan Plateau: An overview. *Earth-Sci. Rev.* **2022**, *234*, 104216. [CrossRef]
18. Liu, Y.Z.; Zhu, Q.Z.; Huang, J.P.; Hua, S.; Jia, R. Impact of dust-polluted convective clouds over the Tibetan Plateau on downstream precipitation. *Atmos. Environ.* **2019**, *209*, 67–77. [CrossRef]
19. Kim, B.; Miller, M.A.; Schwartz, S.E.; Liu, Y.; Min, Q. The role of adiabaticity in the aerosol first indirect effect. *J. Geophys. Res.-Atmos.* **2008**, *113*, D5. [CrossRef]
20. Lihavainen, H.; Kerminen, V.-M.; Remer, L. Aerosol-cloud interaction determined by both in situ and satellite data over a northern high-latitude site. *Atmos. Chem. Phys.* **2010**, *10*, 10987–10995. [CrossRef]
21. Liu, Y.Q.; de Leeuw, G.; Kerminen, V.M.; Zhang, J.H.; Zhou, P.T.; Nie, W.; Qi, X.M.; Hong, J.; Wang, Y.H.; Ding, A.J.; et al. Analysis of aerosol effects on warm clouds over the Yangtze River Delta from multi-sensor satellite observations. *Atmos. Chem. Phys.* **2017**, *17*, 5623–5641. [CrossRef]

22. Pandithurai, G.; Takamura, T.; Yamaguchi, J.; Miyagi, K.; Takano, T.; Ishizaka, Y.; Dipu, S.; Shimizu, A.J.G.R.L. Aerosol effect on cloud droplet size as monitored from surface-based remote sensing over East China Sea region. *Geophys. Res. Lett.* **2009**, *36*, 13. [CrossRef]
23. Wang, F.; Guo, J.P.; Wu, Y.R.; Zhang, X.Y.; Deng, M.J.; Li, X.W.; Zhang, J.H.; Zhao, J. Satellite observed aerosol-induced variability in warm cloud properties under different meteorological conditions over eastern China. *Atmos. Environ.* **2014**, *84*, 122–132. [CrossRef]
24. Zhao, C.; Qiu, Y.; Dong, X.; Wang, Z.; Peng, Y.; Li, B.; Wu, Z.; Wang, Y.J.E.; Science, S. Negative aerosol-cloud re relationship from aircraft observations over Hebei, China. *Earth Space Sci.* **2018**, *5*, 19–29. [CrossRef]
25. Zhao, P.; Zhao, W.; Yuan, L.; Zhou, X.; Ge, F.; Xiao, H.; Zhang, P.; Wang, Y.; Zhou, Y. Spatial heterogeneity of aerosol effect on liquid cloud microphysical properties in the warm season over Tibetan Plateau. *J. Geophys. Res.-Atmos.* **2023**, *128*, e2022JD037738. [CrossRef]
26. Kiran, V.R.; Ratnam, M.V.; Fujiwara, M.; Russchenberg, H.; Wienhold, F.G.; Madhavan, B.L.; Raman, M.R.; Nandan, R.; Raj, S.T.A.; Kumar, A.H.; et al. Balloon-borne aerosol-cloud interaction studies (BACIS): Field campaigns to understand and quantify aerosol effects on clouds. *Atmos. Meas. Tech.* **2022**, *15*, 4709–4734. [CrossRef]
27. Ackerman, A.S.; Toon, O.B.; Hobbs, P.V. Dissipation of marine stratiform clouds and collapse of the marine boundary layer due to the depletion of cloud condensation nuclei by clouds. *Science* **1993**, *262*, 226–229. [CrossRef]
28. Hobbs, P.V. Aerosol-Cloud Interactions. In *International Geophysics*; Hobbs, P.V., Ed.; Academic Press: San Diego, CA, USA, 1993; Volume 54, Chapter 2; pp. 33–73.
29. Fan, J.; Wang, Y.; Rosenfeld, D.; Liu, X. Review of aerosol–cloud interactions: Mechanisms, significance, and challenges. *J. Atmos. Sci.* **2016**, *73*, 4221–4252. [CrossRef]
30. Barahona, D.; Nenes, A. Parameterizing the competition between homogeneous and heterogeneous freezing in ice cloud formation–polydisperse ice nuclei. *Atmos. Chem. Phys.* **2009**, *9*, 5933–5948. [CrossRef]
31. Haag, W.; Kärcher, B. The impact of aerosols and gravity waves on cirrus clouds at midlatitudes. *J. Geophys. Res.-Atmos.* **2004**, *109*, D12. [CrossRef]
32. Mao, F.Y.; Pan, Z.X.; Henderson, D.S.; Wang, W.; Gong, W. Vertically resolved physical and radiative response of ice clouds to aerosols during the Indian summer monsoon season. *Remote Sens. Environ.* **2018**, *216*, 171–182. [CrossRef]
33. Massie, S.T.; Delano, J.; Bardeen, C.G.; Jiang, J.H.; Huang, L. Changes in the shape of cloud ice water content vertical structure due to aerosol variations. *Atmos. Chem. Phys.* **2016**, *16*, 6091–6105. [CrossRef]
34. Lohmann, U.; Feichter, J. Global indirect aerosol effects: A review. *Atmos. Chem. Phys.* **2005**, *5*, 715–737. [CrossRef]
35. Twomey, S. The influence of pollution on the shortwave albedo of clouds. *J. Atmos. Sci.* **1977**, *34*, 1149–1152. [CrossRef]
36. Borys, R.D.; Lowenthal, D.H.; Mitchell, D.L. The relationships among cloud microphysics, chemistry, and precipitation rate in cold mountain clouds. *Atmos. Environ.* **2000**, *34*, 2593–2602. [CrossRef]
37. Lohmann, U. A glaciation indirect aerosol effect caused by soot aerosols. *Geophys. Res. Lett.* **2002**, *29*, 11-11–11-14. [CrossRef]
38. Lowenthal, D.H.; Borys, R.D.; Choularton, T.W.; Bower, K.N.; Flynn, M.J.; Gallagher, M.W. Parameterization of the cloud droplet–sulfate relationship. *Atmos. Environ.* **2004**, *38*, 287–292. [CrossRef]
39. Muhlbauer, A.; Hashino, T.; Xue, L.; Teller, A.; Lohmann, U.; Rasmussen, R.M.; Geresdi, I.; Pan, Z. Intercomparison of aerosol-cloud-precipitation interactions in stratiform orographic mixed-phase clouds. *Atmos. Chem. Phys.* **2010**, *10*, 8173–8196. [CrossRef]
40. Saleeby, S.M.; Cotton, W.R.; Lowenthal, D.; Borys, R.D.; Wetzel, M.A. Influence of cloud condensation nuclei on orographic snowfall. *J. Appl. Meteorol.* **2009**, *48*, 903–922. [CrossRef]
41. Twomey, S.A.; Piepgrass, M.; Wolfe, T. An assessment of the impact of pollution on global cloud albedo. *Tellus B* **1984**, *36*, 356–366. [CrossRef]
42. Zhang, D.; Wang, Z.; Heymsfield, A.; Fan, J.; Liu, D.; Zhao, M. Quantifying the impact of dust on heterogeneous ice generation in midlevel supercooled stratiform clouds. *Geophys. Res. Lett.* **2012**, *39*, L18805. [CrossRef]
43. Yao, T.; Chen, F.; Cui, P.; Ma, Y.; Xu, B.; Zhu, L.; Zhang, F.; Wang, W.; Ai, l.; Yang, X. From Tibetan Plateau to Third Pole and Pan-Third Pole. *Bull. Chin. Acad. Sci.* **2017**, *32*, 924–931. [CrossRef]
44. Chen, D.; Xu, B.; Yao, T.; Guo, Z.; Cui, P.; Chen, F.; Zhang, R.; Zhang, X.; Yili, Z.; Jie, F.; et al. Assessment of past, present and future environmental changes on the Tibetan Plateau. *Chin. Sci. Bull.* **2015**, *60*, 3025–3035.
45. Wu, G.; Duan, A.; Zhang, X.; Liu, Y.; Ma, Y.; Yang, K. Extreme weather and climate changes and its environmental effects over the Tibetan Plateau. *Chin. J. Nat.* **2013**, *35*, 167–171.
46. Pokharel, M.; Guang, J.; Liu, B.; Kang, S.C.; Ma, Y.M.; Holben, B.N.; Xia, X.A.; Xin, J.Y.; Ram, K.; Rupakheti, D.; et al. Aerosol Properties Over Tibetan Plateau from a Decade of AERONET Measurements: Baseline, Types, and Influencing Factors. *J. Geophys. Res.-Atmos.* **2019**, *124*, 13357–13374. [CrossRef]
47. Xu, X.F.; Wu, H.; Yang, X.Y.; Xie, L.F. Distribution and transport characteristics of dust aerosol over Tibetan Plateau and Taklimakan Desert in China using MERRA-2 and CALIPSO data. *Atmos. Environ.* **2020**, *237*, 117670. [CrossRef]
48. DeMott, P.J.; Prenni, A.J.; McMeeking, G.R.; Sullivan, R.C.; Petters, M.D.; Tobo, Y.; Niemand, M.; Möhler, O.; Snider, J.R.; Wang, Z.; et al. Integrating laboratory and field data to quantify the immersion freezing ice nucleation activity of mineral dust particles. *Atmos. Chem. Phys.* **2015**, *15*, 393–409. [CrossRef]
49. Huang, J.; Minnis, P.; Yan, H.; Yi, Y.; Chen, B.; Zhang, L.; Ayers, J.K. Dust aerosol effect on semi-arid climate over Northwest China detected from A-Train satellite measurements. *Atmos. Chem. Phys.* **2010**, *10*, 6863–6872. [CrossRef]

50. Klein, H.; Nickovic, S.; Haunold, W.; Bundke, U.; Nillius, B.; Ebert, M.; Weinbruch, S.; Schuetz, L.; Levin, Z.; Barrie, L.A.; et al. Saharan dust and ice nuclei over Central Europe. *Atmos. Chem. Phys.* **2010**, *10*, 10211–10221. [CrossRef]
51. Liu, D.T.; He, C.L.; Schwarz, J.P.; Wang, X. Lifecycle of light-absorbing carbonaceous aerosols in the atmosphere. *npj Clim. Atmos. Sci.* **2020**, *3*, 40. [CrossRef]
52. Pan, B.W.; Yao, Z.D.; Wang, M.Z.; Pan, H.L.; Bu, L.B.; Kumar, K.R.; Gao, H.Y.; Huang, X.Y. Evaluation and utilization of CloudSat and CALIPSO data to analyze the impact of dust aerosol on the microphysical properties of cirrus over the Tibetan Plateau. *Adv. Space Res.* **2019**, *63*, 2–15. [CrossRef]
53. Pratt, K.A.; DeMott, P.J.; French, J.R.; Wang, Z.; Westphal, D.L.; Heymsfield, A.J.; Twohy, C.H.; Prenni, A.J.; Prather, K.A. In situ detection of biological particles in cloud ice-crystals. *Nat. Geosci.* **2009**, *2*, 397–400. [CrossRef]
54. Wang, W.C.; Sheng, L.F.; Jin, H.C.; Han, Y.Q. Dust aerosol effects on cirrus and altocumulus clouds in Northwest China. *J. Meteorol. Res.* **2015**, *29*, 793–805. [CrossRef]
55. Hua, S. Study on Aerosol-Cloud Interaction and Cloud Radiative Effect over the Tibetan Plateau. Ph.D. Thesis, Lanzhou University, Lanzhou, China, 2020.
56. Hua, S.; Liu, Y.Z.; Luo, R.; Shao, T.B.; Zhu, Q.Z. Inconsistent aerosol indirect effects on water clouds and ice clouds over the Tibetan Plateau. *Int. J. Climatol.* **2020**, *40*, 3832–3848. [CrossRef]
57. Liu, Y.Z.; Hua, S.; Jia, R.; Huang, J.P. Effect of Aerosols on the Ice Cloud Properties Over the Tibetan Plateau. *J. Geophys. Res.-Atmos.* **2019**, *124*, 9594–9608. [CrossRef]
58. Yuan, C.; Yao, X.; Qu, Y.; Chen, T.; Huang, Y.; Ma, J. Variability of clouds over Southeast Tibetan Plateau: The roles of aerosols. *Chin. Sci. Bull.* **2023**, *68*, 532–545. [CrossRef]
59. Liu, Y.Z.; Zhu, Q.Z.; Hua, S.; Alam, K.; Dai, T.; Cheng, Y.M. Tibetan Plateau driven impact of Taklimakan dust on northern rainfall. *Atmos. Environ.* **2020**, *234*, 117583. [CrossRef]
60. Merdji, A.; Xu, X.F.; Lu, C.S.; Habtemicheal, B.A.; Li, J.J. Accuracy assessment and climatology of MODIS aerosol optical properties over North Africa. *Environ. Sci. Pollut. Res.* **2023**, *30*, 13449–13468. [CrossRef] [PubMed]
61. Manenti, F.; Cavazzani, S.; Bertolin, C.; Ortolani, S.; Fiorentin, P. Spatial-Temporal resolution implementation of cloud-aerosols data through satellite cross-correlation. *MethodsX* **2024**, *12*, 102547. [CrossRef] [PubMed]
62. Merdji, A.; Lu, C.S.; Xu, X.F.; Mhawish, A. Long-term three-dimensional distribution and transport of Saharan dust: Observation from CALIPSO, MODIS, and reanalysis data. *Atmos. Res.* **2023**, *286*, 106658. [CrossRef]
63. Pan, Z.X.; Mao, F.Y.; Gong, W.; Min, Q.L.; Wang, W. The warming of Tibetan Plateau enhanced by 3D variation of low-level clouds during daytime. *Remote Sens. Environ.* **2017**, *198*, 363–368. [CrossRef]
64. Winker, D.M.; Pelon, J.; Coakley, J.A.; Ackerman, S.A.; Charlson, R.J.; Colarco, P.R.; Flamant, P.; Fu, Q.; Hoff, R.M.; Kittaka, C.; et al. THE CALIPSO MISSION A Global 3D View of Aerosols and Clouds. *Bull. Am. Meteorol. Soc.* **2010**, *91*, 1211–1229. [CrossRef]
65. Xu, X.; Dong, L.; Zhao, Y.; Wang, Y. Effect of the Asian Water Tower over the Qinghai-Tibet Plateau and the characteristics of atmospheric water circulation. *Chin. Sci. Bull.* **2019**, *64*, 2830–2841.
66. Shen, J.; Cao, N. Characteristics of Aerosol Vertical Distribution over the Yangtze River Delta Region of China in 2018. *Environ. Sci.* **2019**, *40*, 4743–4754. [CrossRef] [PubMed]
67. Omar, A.H.; Winker, D.M.; Tackett, J.L.; Giles, D.M.; Kar, J.; Liu, Z.; Vaughan, M.A.; Powell, K.A.; Trepte, C.R. CALIOP and AERONET aerosol optical depth comparisons: One size fits none. *J. Geophys. Res.-Atmos.* **2013**, *118*, 4748–4766. [CrossRef]
68. Wang, Z.; Sassen, K. Cloud Type and Macrophysical Property Retrieval Using Multiple Remote Sensors. *J. Appl. Meteorol.* **2001**, *40*, 1665–1682. [CrossRef]
69. Zhang, D.; Wang, Z.; Liu, D. A global view of midlevel liquid-layer topped stratiform cloud distribution and phase partition from CALIPSO and CloudSat measurements. *J. Geophys. Res.-Atmos.* **2010**, *115*, D4. [CrossRef]
70. Fang, L.; Li, Y.; Sun, G.; Gao, C.; Lu, Z. Horizontal and Vertical Distributions of Clouds of Different Types Based on CloudSat-CALIPSO Data. *Clim. Environ. Res.* **2016**, *21*, 547–556.
71. Kendall, M.G. Partial Rank correlation. *Biometrika* **1942**, *32*, 277–283. [CrossRef]
72. Zhao, B.; Gu, Y.; Liou, K.N.; Wang, Y.; Liu, X.H.; Huang, L.; Jiang, J.H.; Su, H. Type-Dependent Responses of Ice Cloud Properties to Aerosols From Satellite Retrievals. *Geophys. Res. Lett.* **2018**, *45*, 3297–3306. [CrossRef] [PubMed]
73. Zaman, S.U.; Pavel, M.R.S.; Joy, K.S.; Jeba, F.; Islam, M.S.; Paul, S.; Bari, M.A.; Salam, A. Spatial and temporal variation of aerosol optical depths over six major cities in Bangladesh. *Atmos. Res.* **2021**, *262*, 105803. [CrossRef]
74. Che, H.Z.; Wang, Y.Q.; Sun, J.Y.; Zhang, X.C.; Zhang, X.Y.; Guo, J.P. Variation of Aerosol Optical Properties over the Taklimakan Desert in China. *Aerosol Air Qual. Res.* **2013**, *13*, 777–785. [CrossRef]
75. Liu, D.; Zhao, T.L.; Boiyo, R.; Chen, S.Y.; Lu, Z.Q.; Wu, Y.; Zhao, Y. Vertical Structures of Dust Aerosols over East Asia Based on CALIPSO Retrievals. *Remote Sens.* **2019**, *11*, 701. [CrossRef]
76. Zhen, X.; Kang, Y.; Yang, X.; Yang, F.; He, Q. Statistical Analysis of Dust Weather Frequency in Taklamakan Desert. *Environ. Sci. Manag.* **2021**, *46*, 133–137.
77. Ge, J.M.; Huang, J.P.; Xu, C.P.; Qi, Y.L.; Liu, H.Y. Characteristics of Taklimakan dust emission and distribution: A satellite and reanalysis field perspective. *J. Geophys. Res.-Atmos.* **2014**, *119*, 11772–11783. [CrossRef]

78. Huang, J.P.; Wang, T.H.; Wang, W.C.; Li, Z.Q.; Yan, H.R. Climate effects of dust aerosols over East Asian arid and semiarid regions. *J. Geophys. Res.-Atmos.* **2014**, *119*, 11398–11416. [CrossRef]
79. Froyd, K.D.; Yu, P.F.; Schill, G.P.; Brock, C.A.; Kupc, A.; Williamson, C.J.; Jensen, E.J.; Ray, E.; Rosenlof, K.H.; Bian, H.S.; et al. Dominant role of mineral dust in cirrus cloud formation revealed by global-scale measurements. *Nat. Geosci.* **2022**, *15*, 177. [CrossRef]
80. Shen, H.; Yin, Z.; He, Y.; Wang, L.; Zhan, Y.; Jing, D. Measurement report: Influence of long-range transported dust on cirrus cloud formation over remote ocean: Case studies near Midway Island, Pacific. *EGUsphere* **2023**, *2023*, 1–21. [CrossRef]
81. Xu, C.; Ma, Y.M.; Yang, K.; You, C. Tibetan Plateau Impacts on Global Dust Transport in the Upper Troposphere. *J. Clim.* **2018**, *31*, 4745–4756. [CrossRef]
82. Fossum, K.N.; Ovadnevaite, J.; Ceburnis, D.; Preissler, J.; Snider, J.R.; Huang, R.J.; Zuend, A.; O'Dowd, C. Sea-spray regulates sulfate cloud droplet activation over oceans. *npj Clim. Atmos. Sci.* **2020**, *3*, 14. [CrossRef]
83. Singh, A.; Raj, S.S.; Panda, U.; Kommula, S.M.; Jose, C.; Liu, T.; Huang, S.; Swain, B.; Pöhlker, M.L.; Reyes-Villegas, E. Rapid growth and high cloud-forming potential of anthropogenic sulfate aerosol in a thermal power plant plume during COVID lockdown in India. *npj Clim. Atmos. Sci.* **2023**, *6*, 109. [CrossRef]
84. Wang, T.H.; Han, Y.; Huang, J.P.; Sun, M.X.; Jian, B.D.; Huang, Z.W.; Yan, H.R. Climatology of Dust-Forced Radiative Heating Over the Tibetan Plateau and Its Surroundings. *J. Geophys. Res.-Atmos.* **2020**, *125*, e2020JD032942. [CrossRef]
85. Fan, J.; Leung, L.R.; DeMott, P.J.; Comstock, J.M.; Singh, B.; Rosenfeld, D.; Tomlinson, J.M.; White, A.; Prather, K.A.; Minnis, P.; et al. Aerosol impacts on California winter clouds and precipitation during CalWater 2011: Local pollution versus long-range transported dust. *Atmos. Chem. Phys.* **2014**, *14*, 81–101. [CrossRef]
86. Luo, R.; Liu, Y.Z.; Luo, M.; Li, D.; Tan, Z.Y.; Shao, T.B.; Alam, K. Dust effects on mixed-phase clouds and precipitation during a super dust storm over northern China. *Atmos. Environ.* **2023**, *313*, 120081. [CrossRef]
87. Engström, A.; Ekman, A.M.L. Impact of meteorological factors on the correlation between aerosol optical depth and cloud fraction. *Geophys. Res. Lett.* **2010**, *37*, L18814. [CrossRef]
88. Shao, N.; Lu, C.; Jia, X.; Wang, Y.; Li, Y.; Yin, Y.; Zhu, B.; Zhao, T.; Liu, D.; Niu, S.; et al. Radiation fog properties in two consecutive events under polluted and clean conditions in the Yangtze River Delta, China: A simulation study. *Atmos. Chem. Phys.* **2023**, *23*, 9873–9890. [CrossRef]
89. Yang, Y.; Russell, L.M.; Lou, S.J.; Liu, Y.; Singh, B.; Ghan, S.J. Rain-aerosol relationships influenced by wind speed. *Geophys. Res. Lett.* **2016**, *43*, 2267–2274. [CrossRef]
90. Alam, K.; Anwar, K.; Liu, Y.A.; Huang, Z.W.; Huang, J.P.; Liu, Y.Z. Analysis of aerosol cloud interactions with a consistent signal of meteorology and other influencing parameters. *Atmos. Res.* **2022**, *275*, 106241. [CrossRef]
91. Wang, S.; Zhao, W.X.; Liu, Q.Q.; Zhou, J.C.; Crumeyrolle, S.; Xu, X.Z.; Zhang, C.; Ye, C.X.; Zheng, Y.; Che, H.Z.; et al. Strong Aerosol Absorption and Its Radiative Effects in Lhasa on the Tibetan Plateau. *Geophys. Res. Lett.* **2024**, *51*, e2023GL107833. [CrossRef]
92. Yin, Y.; Chen, L. The effects of heating by transported dust layers on cloud and precipitation: A numerical study. *Atmos. Chem. Phys.* **2007**, *7*, 3497–3505. [CrossRef]
93. Carrió, G.G.; Cotton, W.R.; Cheng, W.Y.Y. Urban growth and aerosol effects on convection over Houston Part I: The August 2000 case. *Atmos. Res.* **2010**, *96*, 560–574. [CrossRef]
94. Han, J.Y.; Baik, J.J.; Khain, A.P. A Numerical Study of Urban Aerosol Impacts on Clouds and Precipitation. *J. Atmos. Sci.* **2012**, *69*, 504–520. [CrossRef]
95. Van Den Heever, S.C.; Cotton, W.R. Urban aerosol impacts on downwind convective storms. *J. Appl. Meteorol. Climatol.* **2007**, *46*, 828–850. [CrossRef]
96. Fan, J.W.; Rosenfeld, D.; Yang, Y.; Zhao, C.; Leung, L.R.; Li, Z.Q. Substantial contribution of anthropogenic air pollution to catastrophic floods in Southwest China. *Geophys. Res. Lett.* **2015**, *42*, 6066–6075. [CrossRef]
97. Ackerman, A.S.; Toon, O.B.; Stevens, D.E.; Heymsfield, A.J.; Ramanathan, V.; Welton, E.J. Reduction of tropical cloudiness by soot. *Science* **2000**, *288*, 1042–1047. [CrossRef]
98. Xiong, C.R.; Li, J.; Liu, Z.X.; Zhang, Z.Y. The dominant role of aerosol-cloud interactions in aerosol-boundary layer feedback: Case studies in three megacities in China. *Front. Environ. Sci.* **2022**, *10*, 1002412. [CrossRef]
99. Seiki, T.; Nakajima, T. Aerosol Effects of the Condensation Process on a Convective Cloud Simulation. *J. Atmos. Sci.* **2014**, *71*, 833–853. [CrossRef]
100. Herbert, R.J.; Bellouin, N.; Highwood, E.J.; Hill, A.A. Diurnal cycle of the semi-direct effect from a persistent absorbing aerosol layer over marine stratocumulus in large-eddy simulations. *Atmos. Chem. Phys.* **2020**, *20*, 1317–1340. [CrossRef]
101. Feingold, G.; Remer, L.A.; Ramaprasad, J.; Kaufman, Y.J. Analysis of smoke impact on clouds in Brazilian biomass burning regions: An extension of Twomey's approach. *J. Geophys. Res.-Atmos.* **2001**, *106*, 22907–22922. [CrossRef]
102. Patel, P.N.; Kumar, R. Dust Induced Changes in Ice Cloud and Cloud Radiative Forcing over a High Altitude Site. *Aerosol Air Qual. Res.* **2016**, *16*, 1820–1831. [CrossRef]

103. Li, X.; Wang, H.; Chakraborty, T.; Sorooshian, A.; Ziemba, L.D.; Voigt, C.; Thornhill, K.L. On the Stochasticity of Aerosol-Cloud Interactions within a Data-driven Framework. *arXiv* **2024**, arXiv:2403.08702.
104. Su, L.; Fung, J.C.H. Investigating the role of dust in ice nucleation within clouds and further effects on the regional weather system over East Asia—Part 1: Model development and validation. *Atmos. Chem. Phys.* **2018**, *18*, 8707–8725. [CrossRef]